

AN EXPERIMENTAL STUDY OF AIR ENTRAINMENT  
IN WEB HANDLING APPLICATIONS

By

MOHAMMAD SOHAIL BASHEER

Bachelor of Engineering

N.E.D University of Engineering & Technology

Karachi, Pakistan

1985

Submitted to the Faculty of the  
Graduate College of the  
Oklahoma State University  
in partial fulfillment of  
the requirements for  
the Degree of  
MASTER OF SCIENCE  
July, 1988



AN EXPERIMENTAL STUDY OF AIR ENTRAINMENT  
IN WEB HANDLING APPLICATIONS

Thesis Approved:

*F. O. Thom*

Thesis Adviser

*J. K. Good*

*John J. Shelton*

*Norman N. Osburn*

Dean of the Graduate College

## PREFACE

I wish to express my sincere gratitude to my advisor, Dr. F. O. Thomas for all the guidance and encouragement during this work and during my stay at Oklahoma State University. I also thank him for involving me in WHRC project and giving me chance to do experimental work and further helping me analyze experimental measurements and in writing this thesis. He has extended such help irrespective of time and place and I am very thankful for that.

I would also like to thank my committee members, Dr. J. Shelton and Dr. K. Good, for their advisement during this study. Special thanks are also due to Ron Wood of Mobil Chemical Company, New York, for providing web materials without which completion of this project would have been impossible. I also thank Web Handling Research Center for the financial support during the course of this work.

I am deeply indebted to my father and mother, Mr. and Mrs. Basheer Uddin and brothers and sisters for their continued prayers, moral support and encouragement.

## TABLE OF CONTENTS

Chapter	Page
I. INTRODUCTION.....	1
1.1. Background.....	1
1.2. Objectives of the Investigation.....	7
II. EXPERIMENTAL FACILITY AND MEASUREMENT TECHNIQUES.....	8
2.1. Test Set-Up.....	9
2.2. Review of Existing Micro-Inch Range Displacement Measuring Techniques.....	15
2.3. The Fotonic Sensor.....	17
2.3.1. Description of the Set-Up Used for the Calibration of the Fotonic Sensor.....	26
2.3.2. Procedure for Determining the Calibration Curve.....	28
2.4. Selection of Web Materials.....	35
2.5. Description of Experiments.....	36
III. EXPERIMENTAL RESULTS AND DISCUSSION.....	37
IV. CONCLUSIONS AND RECOMMENDATIONS.....	72
4/5.1. CONCLUSIONS.....	72
4/5.2. RECOMMENDATIONS.....	74
A SELECTED BIBLIOGRAPHY.....	77
APPENDICES.....	78
APPENDIX A - DESCRIPTION OF THE FIVE ELECTROMECHANICAL GUIDE SYSTEM.....	79
APPENDIX B - DESCRIPTION OF THE CALIBRATION MICROMETER.....	82
APPENDIX C - SPECIFICATIONS OF THE WEB MATERIAL.....	88

Chapter

Page

APPENDIX D - COMPUTER PROGRAM LISTINGS.....92

LIST OF TABLES

Table	Page
I. Specifications of MTI-3808R Fotonic Sensor with MTI KD-LS-2A Lens System.....	25
II. Specifications of White Polypropylene Web as Provided by the Manufacturer.....	90
III. Specifications of Metallized Web as Provided by the Manufacturer.....	91

## LIST OF FIGURES

Figure	Page
1. Schematic of Web-Air-Roller Interaction.....	2
2. Schematic of Winding Mechanism.....	4
3. Basic Test Set-Up ( $\beta=20^\circ$ ).....	10
4. Plexiglass Roller Mounted on Brackets.....	11
5. Schematic of Web-Moving Machine.....	12
6. Drive and Tensioning Roller of Web-Moving Machine (A: Drive Roller, B: Tensioning Roller, C: Pointer for Tension Adjustment).....	14
7. The Fotonic Sensor.....	18
8. Schematic of Direct Reflecting Type Fiber Optic Displacement Transducer.....	19
9. Fiber-Optic Displacement Sensor-Lens Imaging Type.....	21
10. Typical Calibration Curves for Direct Reflective Type and Lens Imaging Type.....	23
11. Calibration Micrometer with Probe Holding Fixture.....	27
12. Lateral Probe Traversing Mechanism.....	29
13. Azimuthal Probe Traversing Mechanism.....	30
14. Set-Up During Measurements.....	31
15. Typical Calibration Curve for White Polypropylene Web.....	33
16. Typical Calibration Curve for Metallized Web.....	34

Figure	Page
17. Effect of Velocity and Tension on Air Film Thickness in Constant Gap Region (White Polypropylene Web).....	40
18. Effect of Velocity on Air Film Thickness in Constant Gap Region (Metallized Web).....	41
19. Curved Fitted Experimental Data (White Polypropylene Web).....	43
20. Curved Fitted Experimental Data (Metallized Web).....	44
21. Modified Test Set-Up for High Wrap Angle ( $\beta=60^\circ$ ).....	46
22. Azimuthal Variation in Air Film Thickness ( $y/b=0$ , White Polypropylene Web).....	47
23. Azimuthal Variation in Air Film Thickness ( $y/b=0$ , Metallized Web).....	48
24. Lateral Variation in Air Film Thickness ( $\phi=0^\circ$ , Metallized Web).....	50
25. Lateral Variation in Air Film Thickness ( $\phi=0^\circ$ , White Polypropylene Web).....	52
26. Effect of Grooved Roller Surface On Air Film Thickness.....	54
27. View of Worn-edge Metallized Web.....	55
28. Schematic of Finite Width Effect.....	57
29. Lateral Flow Along with Imposed Boundary Conditions.....	60
30. Velocity Variation Along the Width of the Web.....	62
31. Pressure Variation Along the Width of the Web.....	64
32. Comparison of Experimental Data with Equation (3.20) (White Polypropylene Web).....	66
33. Comparison of Experimental Data with Equation (3.20) (Metallized Web).....	67



Figure	Page
34. Lateral RMS Fluctuation of Air Film Thickness in Constant Gap Region (Metallized Web).....	69
35. Lateral RMS Fluctuation of Air Film Thickness in Constant Gap Region (White Polypropylene Web).....	70
36. Photograph of Web-Moving Machine.....	81
37. Photograph of Calibration Micrometer.....	84
38. Main Slider Block.....	85
39. V-Shaped Rectangular Block.....	86
40. Slider Key with Tapered Slot.....	87

## NOMENCLATURE

A, B, C, D, E	- Coefficients defined by Equation (3.20)
b	- Half width of the web
E	- Modulus of elasticity of the web material
h	- Instantaneous local air film thickness
$h_0$	- Air film thickness in constant gap region
$\bar{h}_0$	- Mean air film thickness in constant gap region
$\bar{h}$	- Mean local air film thickness
$H = \bar{h} / \bar{h}_0$	- Normalized air film thickness
I	- Moment of inertia
P	- Pressure in lubricating air film
$P_a$	- Ambient pressure
$P_{c.g}$	- Air film pressure in constant gap region
r	- Radius of the cylinder substended by inner surface of the web along the arc of web
R1	- Radius of the cylinder substended by the outer surface of the web along the arc of web
R	- Radius of the roller
s	- Web arc length
S	- Constant defined by equation (3.15)

T	- Effective or reduced tension in the web
$T_0$	- Applied tension
U	- Vectorial sum of the web and the roller velocities
$V_{MAX}$	- Lateral velocity of the air at $z=h/2$
$V_{\infty}$	- Lateral velocity of the air at the outer edges of the web
z	- Deformation of the web from the cylinder $r=R+h_0$ along Z-axis
Y	- Coordinate along the width of the web
X	- Coordinate along the length of the web
Z	- Coordinate normal to X and Y axes
u,v,w	- Components of velocity of air
$\beta$	- Total wrap angle
$\Phi$	- Coordinate along the angle of wrap of the web
$\mu$	- Dynamic viscosity of air
$\nu$	- Kinematic viscosity of air
$\theta$	- Normalized X-Coordinate
$\rho$	- Mass density of air
$\sigma$	- Mass per unit area of the web

## CHAPTER I

### INTRODUCTION

#### 1.1 Background

A web is defined as a material which is manufactured in continuous strip form. This definition of web covers a wide range of products such as plastic films, papers, woven and non-woven fabrics of any kind of fiber, magnetic tapes as well as metals.

In the fabrication and handling of plastics, papers, textiles and sheet metals, moving webs are often supported and guided over rollers as shown schematically in Figure 1. In such continuous processing systems, the interaction of the web and the supporting roller has a considerable effect on the overall dynamic performance of the system. Due to the small but non-zero viscosity of air, as the web moves over a supporting roller, air is entrained into the nip region (as shown in Figure 1) and becomes trapped between the web and the roller. The amount of air entrained is of paramount importance in determining the dynamic coefficient of friction between web and roller and in guiding and transporting the web along the process line. It also affects the quality of

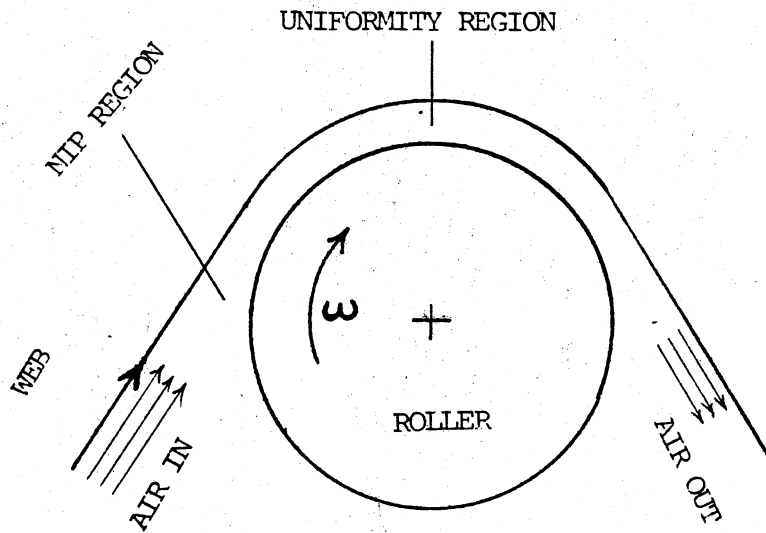


Figure 1. Schematic of Web-Air-Roller Interaction

the web material being processed.

When a large amount of air is entrained, there is little surface contact between the web and the roller even at large asperities. The web rides completely on air and small transversely directed disturbances are not strongly resisted, which causes problems in guiding and tracking the web along the process line. On the contrary, when small amounts of air are brought in, the incoming web contacts the roller at many places. The dynamic coefficient of friction between roller and web is then increased because of the large surface-to-surface contact area. This affects the longitudinal transmission of tension along the process line. Consequently, the web may be scratched and abraded. When the optimum amount of air is trapped, the air gap thickness along with the surface roughness of the film is sufficient to permit a controlled degree of surface-to-surface contact. Transversely directed disturbances can be resisted and smooth longitudinal transmission of tension can be accomplished. Both of these factors help in guiding and transporting the web along the process line.

Similar air entrainment phenomena are also present during winding, the process by which a flat web material is wrapped into round rolls as shown schematically in Figure 2. Here also when a large amount of air is entrained, the area of contact between successive layers of material is reduced, resulting in low inter-layer

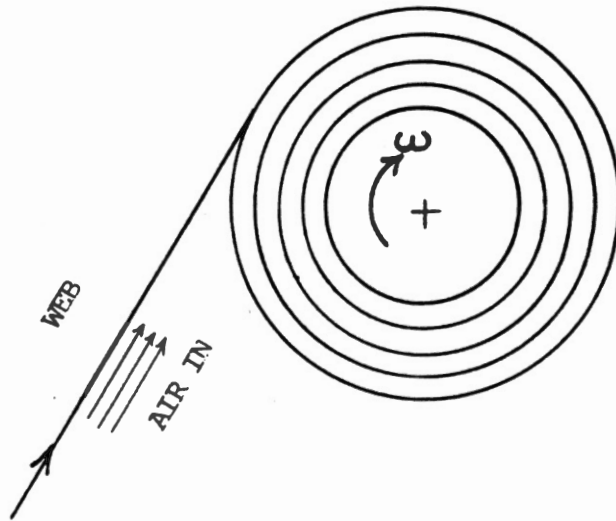


Figure 2. Schematic of Winding Mechanism

pressure. Hence resistance to transversely directed disturbances is small and may lead to failure of roll formation due to "telescoping". On the contrary, if a small amount of air is entrained, the dynamic coefficient of friction between adjacent layers of material is then increased. This can result in a non-uniform distribution of wound-in-tension. Absence of a sufficient amount of air in a wound roll also prevents the smoothing of minor irregularities and promotes the outward propagation of the irregularities as the roll grows, which can locally yield the material.

From the foregoing discussion, the importance of the web-air-roller interaction can be easily recognized. In spite of this, at present there is no complete theory having a sound data base in open literature which allows such an interaction to be accurately predicted. Some insight regarding air entrainment in winding applications can be obtained from Knox & Sweeney (1971). The authors suggested the application of foil bearing theory to model air entrainment effects in winding because of the geometrical similarity between the two problems. The most complete model of fluid effects in web handling applications was presented by Tajuddin (1987). In this work, a model was obtained for predicting air film thickness for the geometry shown in Figure 1 from first principles. The model indicates that the web-air-roller interaction phenomena is governed by the third



order non-linear ordinary differential equation:

$$\frac{d^3H}{d^3\theta} = \frac{1 - H}{H^3} \quad (1.1)$$

Where H is the non-dimensional air gap thickness between the web and the roller and  $\theta$  is a non-dimensional distance along the length of the web.

This governing equation was obtained by simultaneously solving a simplified form of Reynold's hydrodynamic lubrication equation and the web dynamic equilibrium equation. The major assumptions made in deriving the above governing equation are: (1) Perfectly flexible web, (2) Infinitely wide web and (3) Fluid inertial terms are negligible as compared to the viscous terms. The model indicates that air entrainment depends on the sum of the tangential velocity of the roller and the speed of the moving web, tension in the web, radius of the roller and the viscosity of the air. In particular, the relationship obtained by Tajuddin (1987) for the air gap thickness in uniformity region is,

$$h_0 = 0.643R(6\mu U/T)^{2/3} \quad (1.2)$$

Where  $h_0$  is the air gap thickness in the uniformity region (as shown in Figure 1), R is the radius of the roller,  $\mu$  is the dynamic viscosity of the air, U is the sum of the line velocity of the web and the tangential velocity of the roller and T is the reduced or effective

tension in the web defined as follows:

$$T = T_0 - \sigma U^2 \quad (1.3)$$

Where  $T_0$  is the applied tension in pounds per lineal inch and  $\sigma$  is the mass per unit area of the web.

## 1.2 Objectives of the Investigation

It may be concluded from the foregoing discussion that there is a strong need for predicting the amount of air entrained between a web and roller in almost every web handling application. It is also apparent that accurate prediction of entrained air is pre-requisite to any attempt to control or manipulate the amount of entrained air. Based upon the previous discussion, the primary objectives of this study are: (1) To experimentally validate the mathematical model of air entrainment presented by Tajuddin (1987) and to determine how restrictive the assumptions are. (2) Additional understanding of the air entrainment mechanism was sought by measuring for the first time: (a) The spatial variations in air gap thickness along the width as well as along the angle of wrap of the web and (b) The temporal variations in air gap thickness along the width of the web.

## CHAPTER II

### EXPERIMENTAL FACILITY AND MEASUREMENT TECHNIQUES

The present investigation is directed primarily towards experimentally validating the mathematical model of air entrainment presented by Tajuddin (1987). It is therefore desirable that the experimental facility should physically duplicate the essential geometry of a web over a supporting roller (i.e the geometry of Figure 1). In describing the experimental apparatus it is appropriate for the reader to have some idea regarding the order of magnitude of the air gap thickness expected for a typical set of operating conditions. As an example consider 1  $\text{lb}_f/\text{in}$  as the effective or reduced tension per unit width in a web moving at a velocity of 100 in/sec (500 fpm) over a stationary roller of 2 inch radius. Assuming the air to have a dynamic viscosity of  $2.65 \times 10^{-9} \text{ lb}_f\text{-sec}/\text{in}^2$ , equation (1.2) will predict an air gap thickness in uniformity region of 175 micro inches. This example indicates that the air films to be encountered in the measurements set rigorous demands on the experimental set-up and requires a scheme for the measurement of very small web displacements. This chapter will be

devoted to the description of the experimental facility and associated measurement techniques.

### 2.1 Test Set-Up

The basic element of the experimental facility is a flexible web under tension passing over a supporting roller as shown in Figure 3. Keeping in mind that the measurement of the small displacements expected to be encountered in this study is extremely difficult, since the displacement is of the order of 100 micro inches, it was decided to measure the air gap thickness over an 8-inch plexiglass non-rotating roller. The roller was designed to be stationary during experimentation in order to avoid the problems associated with the run-out of a rotating roller and the unavoidable small scale stochastic oscillations in the roller ball bearings.

The plexiglass roller was then mounted securely between two precisely machined brackets on a flat-bed, as shown in Figure 4, so that it will remain rigid during experimentation. Since the roller is stationary, the web is the only moving component in the test set-up. The test cell was then mounted on a continuous loop web-moving machine which provides an angular contact between the web and the roller of approximately 20 degrees and it is shown schematically in Figure 5. The continuous loop web-moving machine is described next.

A continuous loop web-moving machine as shown

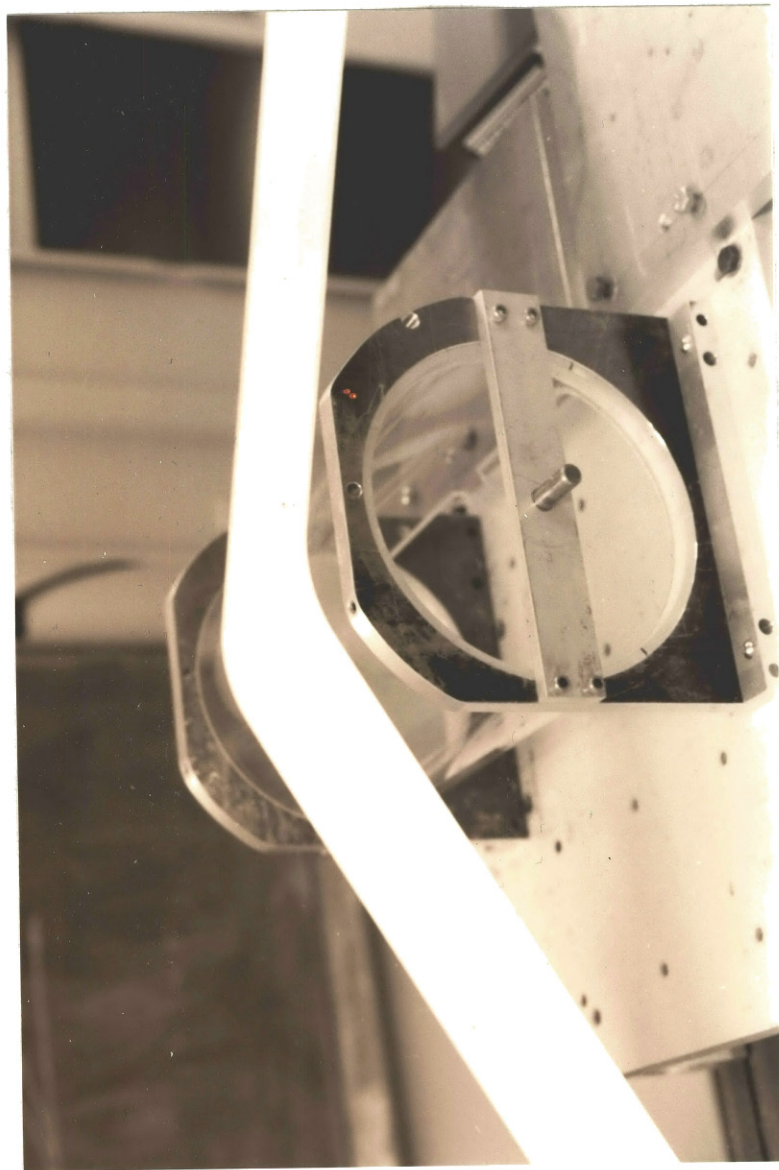


Figure 3. Basic Test Set-Up ( $\beta=20^\circ$ )

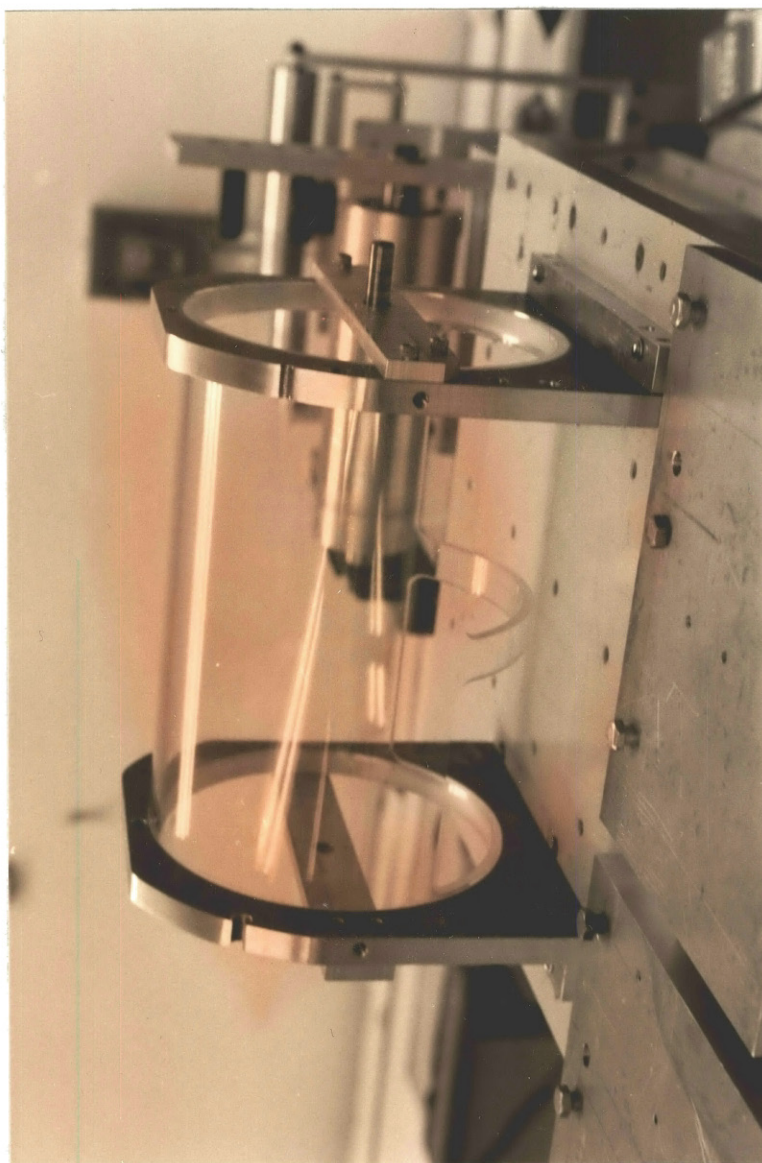


Figure 4. Plexiglass Roller Mounted on Brackets

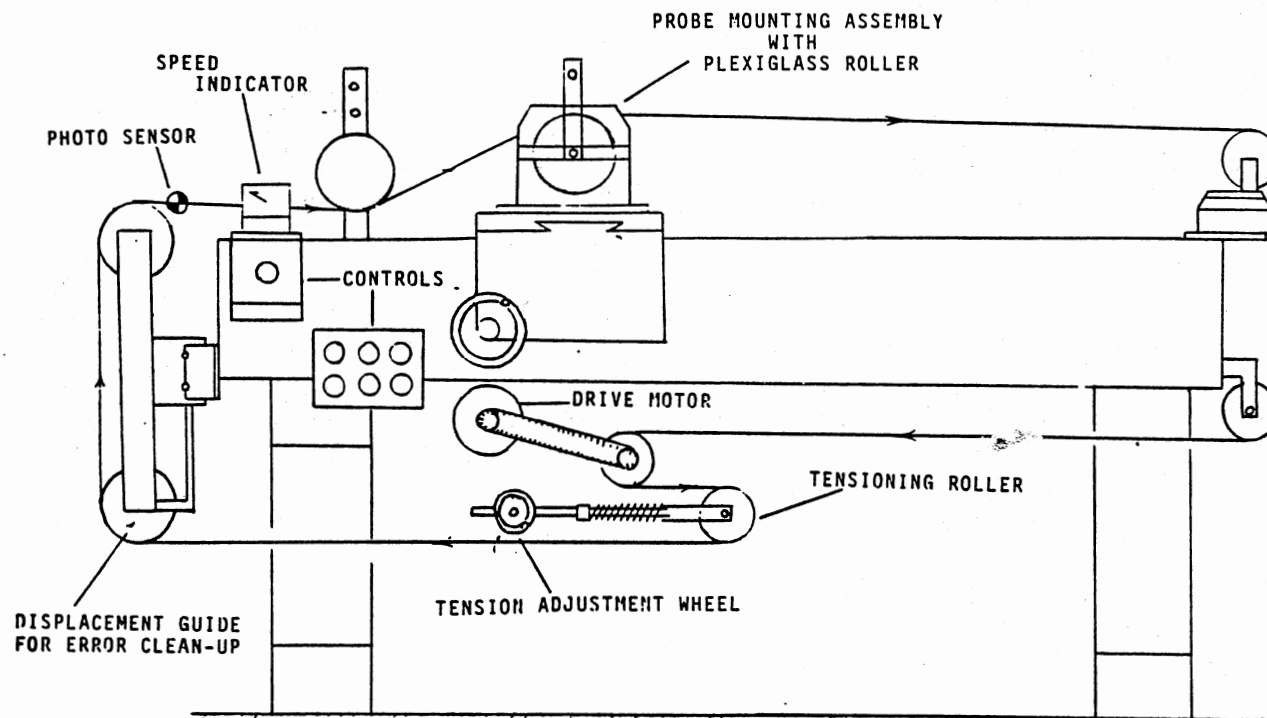


Figure 5. Schematic of Web-Moving Machine

schematically in Figure 5 was used for the experimental study. This web-moving machine has a back-bone type structure, so that a straight reference would be available for precise alignment of the components. It has been constructed from a lathe-bed which was replaned and hand scraped to accomodate the basic test set-up. It has a combination of cantilevered and side mounted rollers which facilitates the changing of the web. The web-moving machine is capable of running at speeds approximately to 250 in/sec (1250 fpm). Power is supplied by an SCR - controlled constant speed drive with tachometer feedback. The drive motor provides enough torque to maintain a constant web velocity during testing. The motor is connected to a voltmeter via a tachometer, and the output is calibrated by a multi-turn potentiometer, so that it reads in fpm. The rubber-covered drive roller as shown in section A of Figure 6 is belted to drive motor. Tension is applied to the web by means of a tensioning roller as shown in section B of Figure 6. A hand crank on the side of the web-moving machine is coupled to a screw through bevel gears which loads two springs against the floating tension roller. The floating tension roller is accurately aligned by tandem ball bushings on hardened and ground stainless steel rods. Tension is adjusted to desired amounts by the pointer and scale arrangement as shown in section C of Figure 6.

In order to guide the moving web along the precise



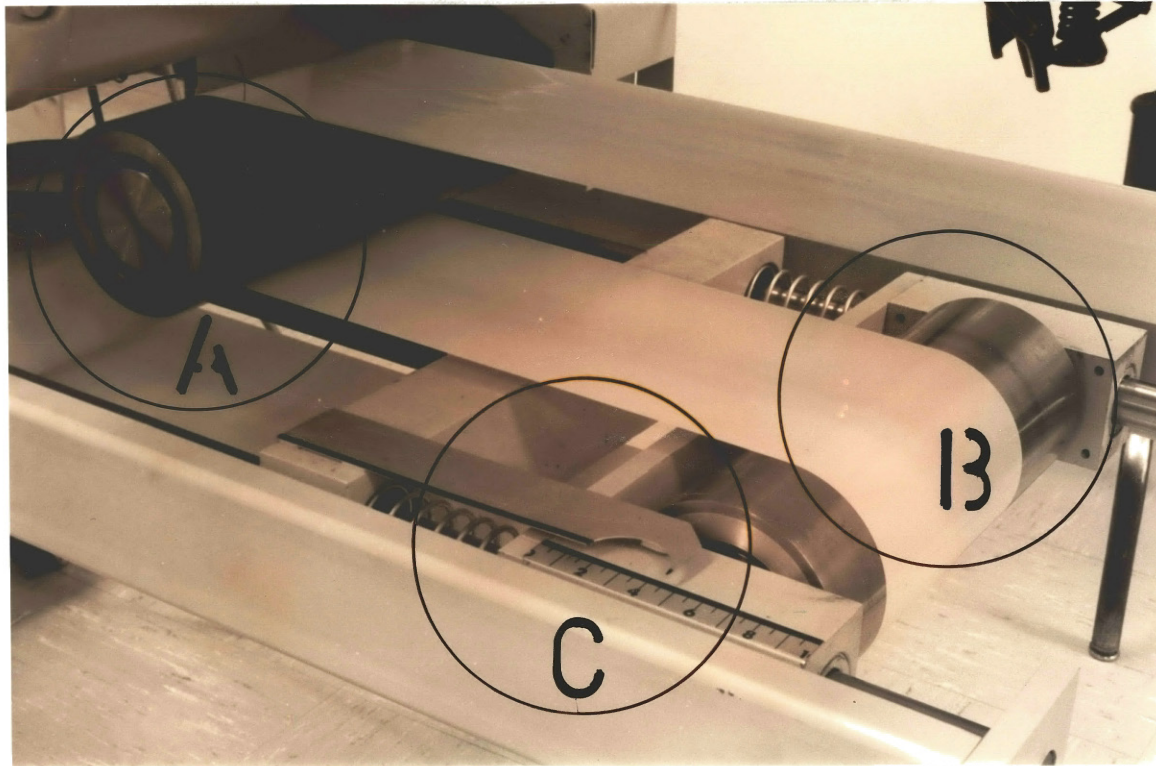


Figure 6. Drive and Tensioning Roller of Web-Moving Machine (A: Drive Roller, B: Tensioning Roller, C: Pointer for Tension Adjustment)

lateral boundaries, the web-moving machine employs the Fife electro-mechanical guiding system as shown on the left side of Figure 5. The guiding system utilizes Fife A9 signal processor, one infra-red sensor, an electro-mechanical actuator and a guide structure. Details of the guider are presented in Appendix A.

The next section will discuss the most crucial link in the present experimental study, i.e. the selection of the measuring technique for determining very small displacements of the web from the roller surface (i.e the air gap thickness).

## 2.2 Review Of Existing Microinch-Range Displacement Measuring Techniques

For any given application, selection of measurement technique is usually affected by the combined impact of simplicity, reliability and geometrical and physical compatibility with the measured system, provided that the probe is capable of the resolution, range and the frequency response required.

Based on the above criteria, three techniques of high precision microinch-range displacement sensing were investigated. These are summarized as follows:

1. High precision displacement sensing using light has traditionally centered around wave interference technique of the Michelson type. However, this technique

requires a very high degree of alignment between the components and also the resolution of such systems is typically on the order of one-eighth of a wavelength of the light used to illuminate the interferometer. Hence, this technique was not practical for the current experimental study because perfect alignment of a moving web with the other optical components in the system was impossible.

2. Measurement techniques using capacitance transducer as the displacement sensing element require a highly conductive web surface (i.e a metallized web), since it works on the principle of varying capacitance. As most of the industrial applications uses a non-metallized web, the use of capacitance transducer will limit the range of web materials. So, this technique is too restrictive.

3. Microinch-range displacement sensing utilizing the Fotonic sensor overcomes the above two limitations, since a) it does not operate on the principle of interference of monochromatic or coherent light, thus the alignment requirements are not so stringent. b) It is equally sensitive to conductive surfaces and non-conductive surfaces since it works on the principle of a reflected light intensity-inverse square law. In addition to this, it has simplicity, small size, mobility, wide frequency capability, extremely small displacement detection limit, very high resolution in the present

measurement range and also possesses the ability to perform without contacting or directly affecting the web surface.

For these reasons, the Fotonic sensor was selected for the experimental work to be reported. Details regarding the Fotonic sensor will be presented in the next section.

### 2.3 The Fotonic Sensor

The Fotonic sensor as shown in Figure 7 is manufactured by the instruments division of MTI, New York. Its principle of operation is next described.

A standard, direct-reflecting type, fiber optic displacement transducer as shown in Figure 8 consists of a set of active and passive optical components. The active components are represented here by the light source and photo sensing element. The passive component is the bifurcated or split bundle of transmit and receive fibers that is physically separated at one end into two separate fiber bundles. All fibers are individually clad to prevent the optical cross talk. The transmit and receive fibers are dispersed randomly throughout the cross section of the probe tip.

In normal use, the probe tip is placed in close proximity to the target surface. Light from the source traveling down the transmitting fibers is reflected from the target surface back onto the receive fibers in the



Figure 7. The Fotonic Sensor

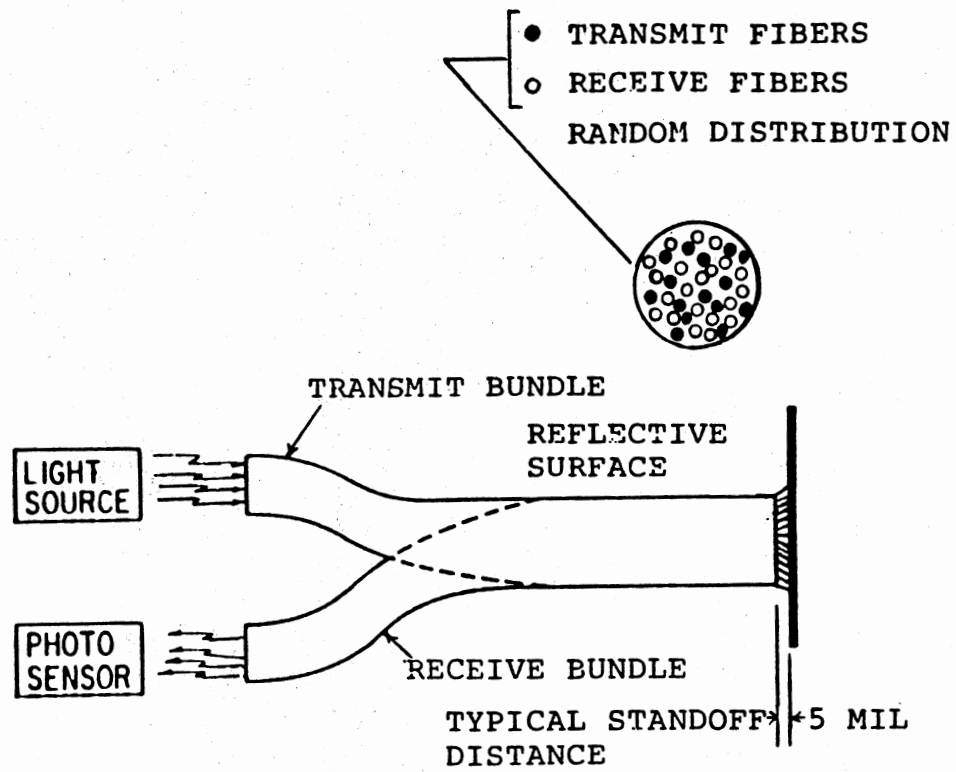


Figure 8. Schematic of Direct Reflecting Type Fiber Optic Displacement Transducer

probe tip and is then detected by a photo sensor. The intensity of the reflected light is related to the distance between the probe tip and the reflective surface, the numerical aperture of the receive fibers (i.e the acceptance angle) and the reflectivity of the target surface. For any probe and target surface, assuming that the acceptance angle of fibers and the reflectivity of target surface remains constant (both are generally true), as the distance between probe and target changes, the probe output voltage also changes in accordance with the light intensity-inverse square law. Thus a calibration curve can be obtained between the probe output in volts and the corresponding probe-to-target distance.

$$V_0 \propto \frac{1}{R^2}$$

For the current experimental study, a new feature was added to the primitive Fotonic sensor configuration. This consisted of a high resolution compound lens system (called KD-LS-2A) manufactured by MTI New York, which was inserted between the Fotonic sensor and the reflective target surface as shown schematically in Figure 9. The major advantage of this design is the increased standoff distance obtained by the use of the lens system. The standoff distance is increased approximately 100 times over the direct reflective type. The exact standoff distance is a function of the focal length of the lens system chosen for imaging. Use of the lens system also increases the sensitivity of the probe by four times.

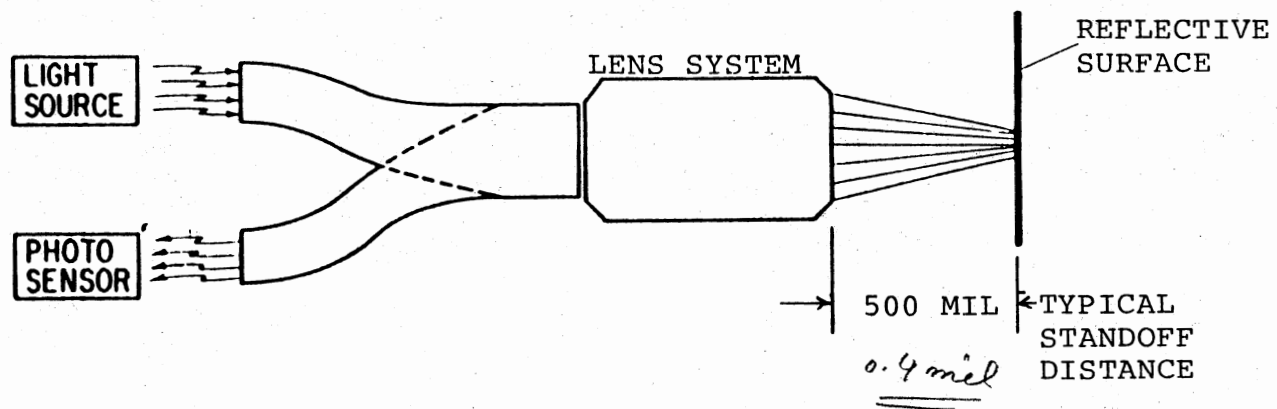


Figure 9. Fiber Optic Displacement Sensor-  
Lens Imaging Type



A qualitative comparison of typical calibration curves between the direct reflective type Fotonic sensor operation and with the lens imaging design is shown in Figure 10. The output intensities of the curves shown in Figure 10 were normalized to the same peak value in order that relative variations in intensity with displacement could be observed directly. The direct reflective type has a peak output at approximately 20 mils displacement from the target surface. The next paragraph will discuss some interesting features about Figure 10.

The right half of the resultant output of a lens imaging system is nearly identical to the direct reflective type except that it occurs at a much larger standoff distance. The reference point of the lens imaging design is where the face of the distal end of the fiber optic bundle is focused and imaged on the reflective target surface. A sharp null occurs in the output of the probe at this point. Two intensity displacement curves (one reversed) that are nearly identical to the output of the direct reflective type occur on either side of this null. This occurs since the bright fiber image of the target is retransmitted back through the lens system along the precise lines from which it came. The ends of the transmit fibers are re-imaged onto themselves (within the accuracy of the lenses employed and the surface finish of the target) and therefore do not provide light to any of the adjacent

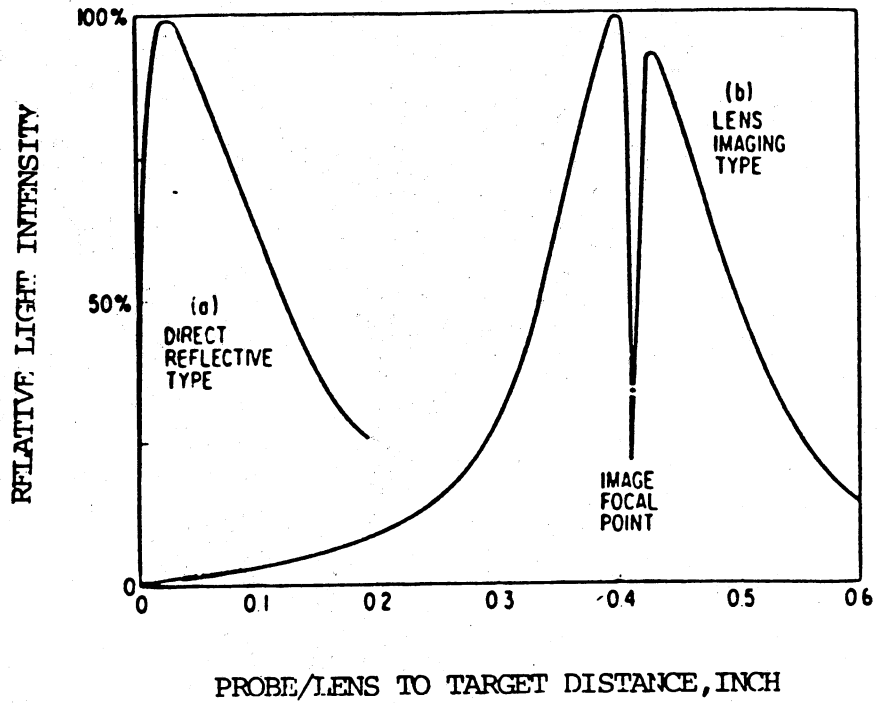


Figure 10. Typical Calibration Curves  
for Direct Reflective Type  
and Lens Imaging Type

receive fibers in the array--thus, an output null at image focus. On either side of the focal point, the primary target image and the retransmitted (secondary) image is blurred, allowing portions of the retransmitted light to fall onto the receive fibers. A peak in output intensity as picked up by the receive fibers occurs on either side of the null due to defocussing. The limitation of performance of the Fotonic sensor is defined by the transmission efficiency of the optical fibers and the limits of resolution of photodetector.

The Fotonic sensor used for the current experimental work was the MTI-3808R. Its principle of operation is the same as discussed above with the addition that the light reflected into the receive fibers of the probe falls on a light sensitive diode. The diode is connected to an amplifier that operates as a current-to-voltage converter. This voltage is proportional to the received light intensity. A filter range switch is also provided which connects the probe to a low pass filter in order to improve the signal to noise ratio by attenuating the instrument response to frequencies above the target frequency. The related specifications of MTI-3808R as provided by the manufacturer are provided in Table I.

It can be easily recognized from the foregoing discussion that the Fotonic sensor employs an indirect method of measuring displacement where the probe output in volts recorded from a process is referred back to an

TABLE I  
SPECIFICATIONS OF MTI-3808R FOTONIC  
SENSR OPERATED WITH AN MTI  
KD-LS-2A LENS SYSTEM

---

Probe Tip Diameter	0.063
Probe Length	36.0
Image Spot Size	0.012
Frequency Response (-3 db) (KHz)	60.0
Standoff	0.390
Sensitivity (uin/mV)	0.16

---

\* All dimensions in inches

already obtained calibration curve (with nearly the same environment) in order to relate it to a corresponding displacement value. Considering the order of magnitude of the required measurements and the resolution required, it was decided to perform an in-situ calibration.

### 2.3.1 Description of the Set-Up Used for the Calibration of the Fotonic Sensor

The Fotonic Sensor used in this experimentation was supplied with a calibration curve from the manufacturer. In-situ calibration was needed however, since the calibration curve supplied by the manufacturer was obtained by using stainless steel target which possesses very different reflective characteristics than the webs to be used in the experiments.

A combination calibration micrometer and lead in probe holding fixture was manufactured and assembled at an on-campus facility and is shown in Figure 11. The set-up was made precise and rigid enough so that the probe can measure very minute displacements of the web with accuracy and repeatability. This calibration micrometer has been machined such that a  $90^{\circ}$  rotation of the positioning screw (shown in Figure 11) will cause the probe to move 0.0001 inches towards or away from the web surface. The calibration micrometer along with its components is discussed in detail in Appendix B.

In order to scan the air gap thickness along the

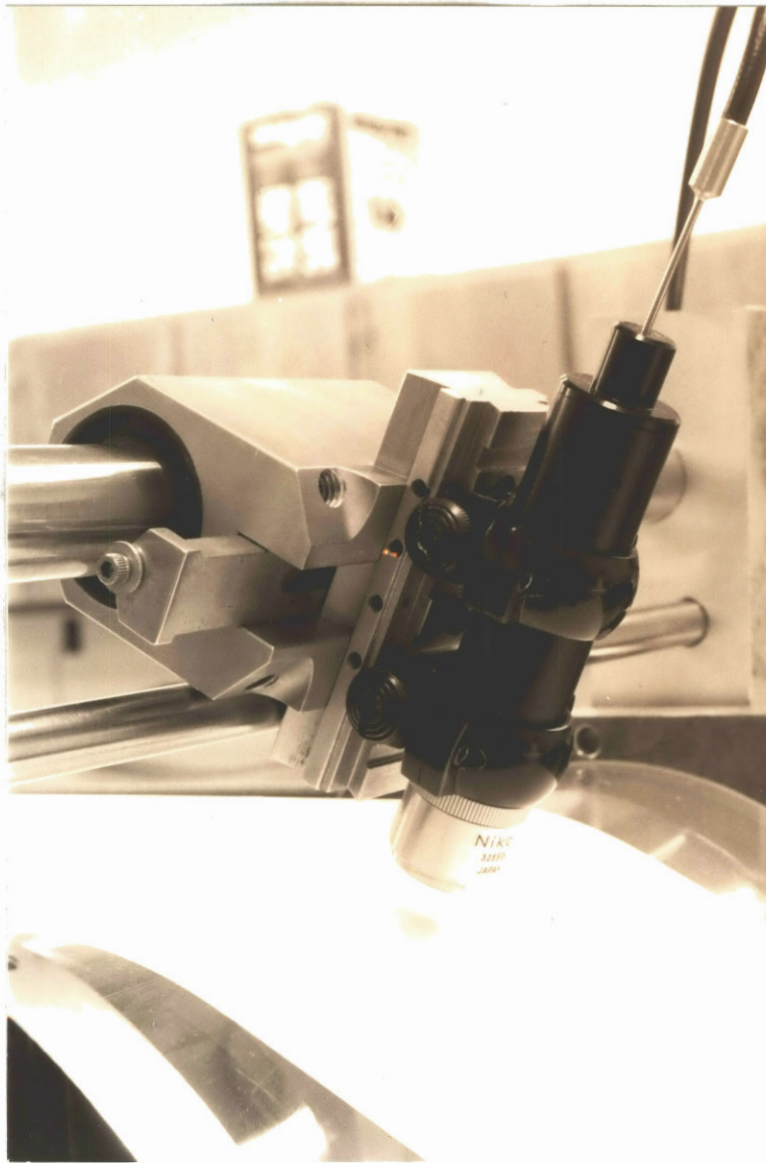


Figure 11. Calibration Micrometer with  
Probe holding Fixture

width of the web, the main slider block was allowed to slide on a one-inch diameter ground and hardened stainless steel rod as shown in Figures 12, where it can be fixed at any desired position.

To scan the air gap thickness along the angle of wrap of web, the whole mechanism can be moved and readjusted at any desired angular position as shown in Figures 13.

In addition to the above, Fotonic sensor was also used for the accurate measurement of the web velocity. The Fotonic sensor output shows a strong discontinuity whenever splice (an overlapping joint of web material to form a continuous web) on the web surface passes across it. The time delay between two such discontinuities will be the time period of the web motion. The inverse of this time period when multiplied by the length of the web will give an accurate measurement of the web velocity.

### 2.3.2 Procedure for Determining the Calibration Curve

The calibration is done at a location where the air gap thickness is to be measured as shown in Figure 14. Before any measurements were taken, the instruments were allowed sufficient time to reach steady state in order to reduce any amplifier drift. Appropriate intensity levels were set for the sensor light in order to avoid any overshoot or under-shoot of probe output during calibration.

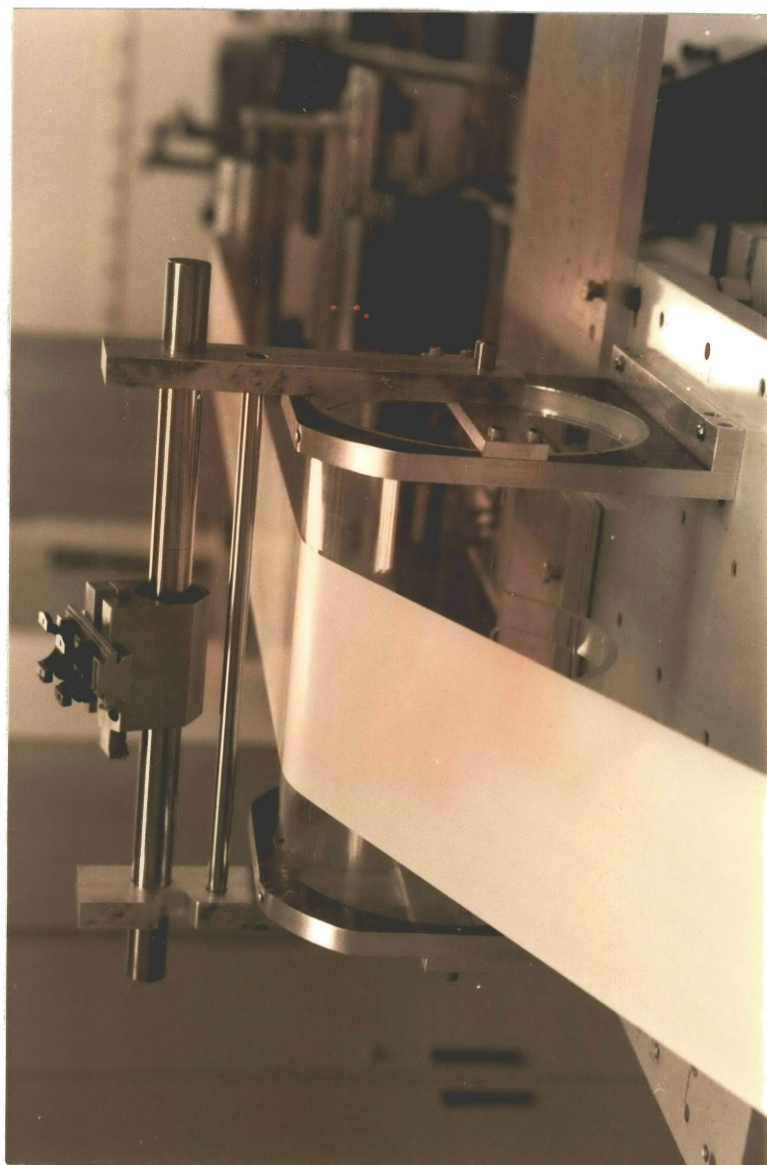


Figure 12. Lateral Probe Traversing Mechanism



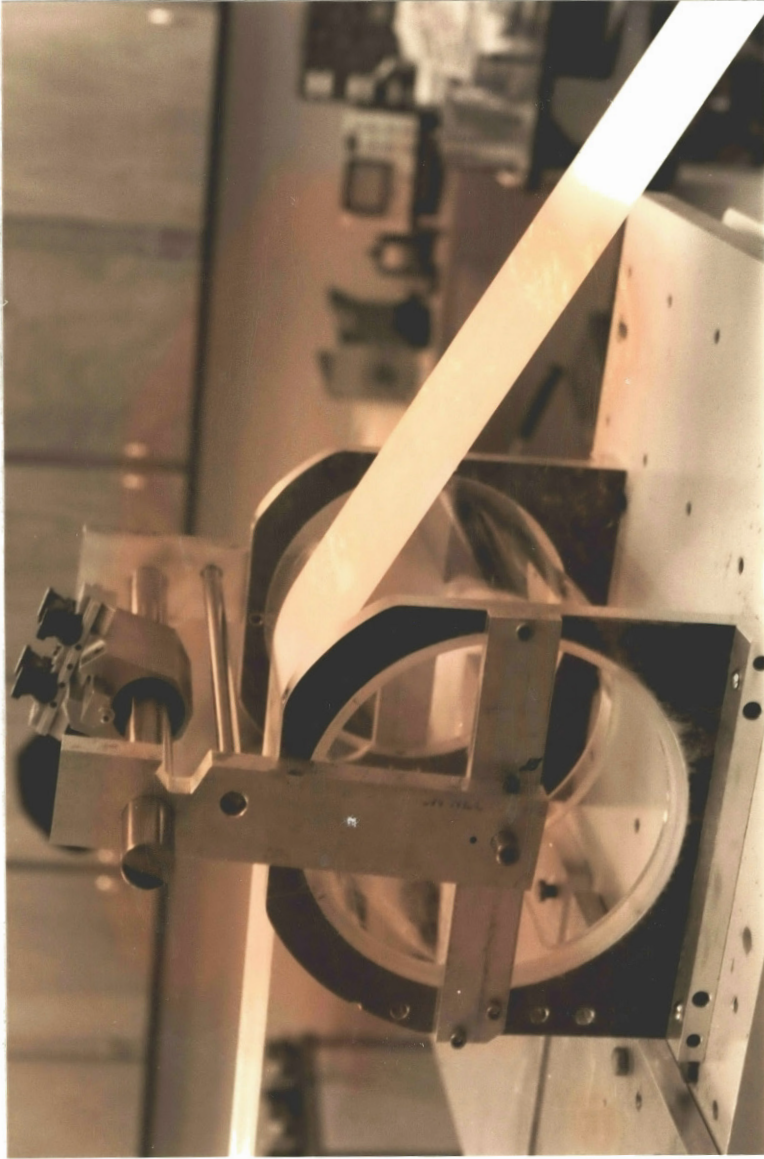


Figure 13. Azimuthal Probe Traversing Mechanism

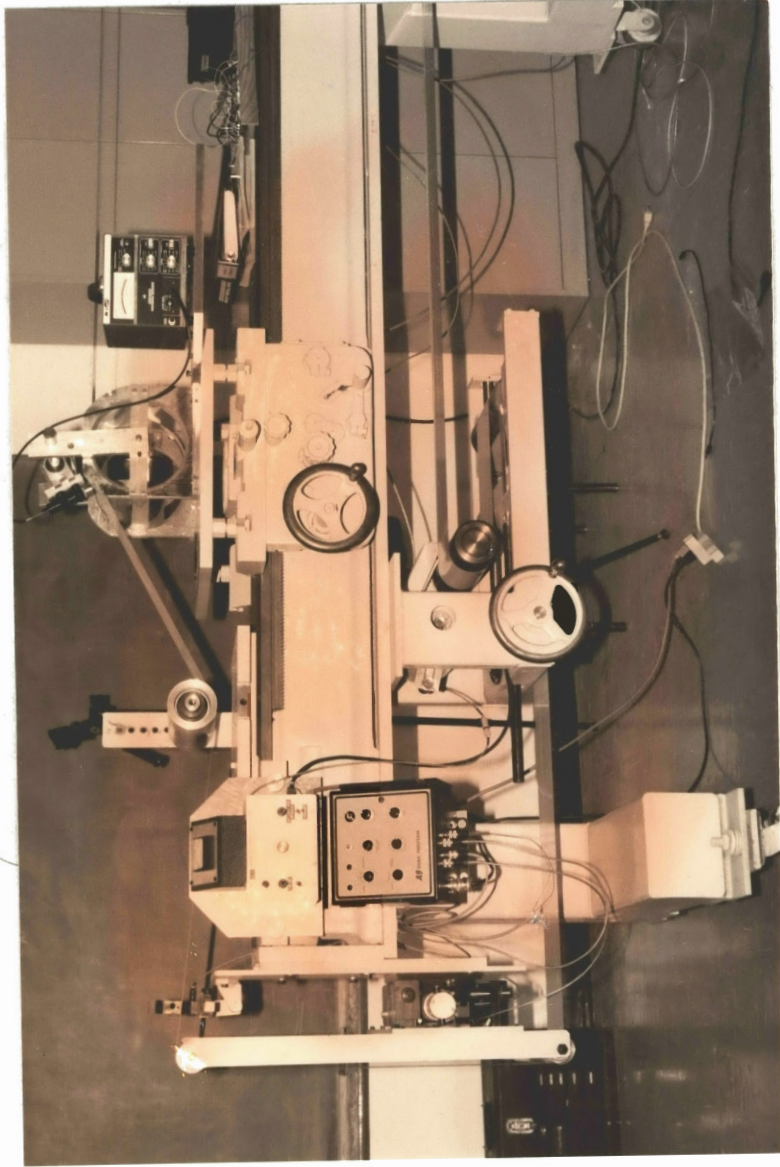


Figure 14. Set-Up During Measurements

The probe's low-pass cut-off frequency limit was then adjusted in order to have good signal-to-noise ratio. For data acquisition purposes, the analog output from Fotonic sensor was digitized and stored on-line with the help of 12-bit DT 2805 A/D board, which was installed in TI-portable computer. The data sampling frequency in all cases was 800 Hz and was selected in conformance with the Nyquist criterion, which demands that the signal sampling frequency should be at least twice the maximum anticipated frequency in the signal.

Initially, the distance between the probe and the stationary taut web was roughly adjusted so that it approximately gives a focused image of the probe tip on the web surface while the probe is looking perpendicularly at the web as shown in Figure 14. Then, by indexing the screw on the slider-key, the probe was allowed to move towards the web surface in known but very small increments while the resulting output voltages were recorded. In this manner a calibration curve was obtained between the Fotonic sensor output in volts and the distance of the probe from the web target surface. Typical calibration curves for White Polypropylene and metallic webs used for the experimental work are shown in Figures 15 and 16 respectively.

From the calibration curves, it is obvious that the probe is very sensitive between points A and B for both the web materials. It was desired to employ most

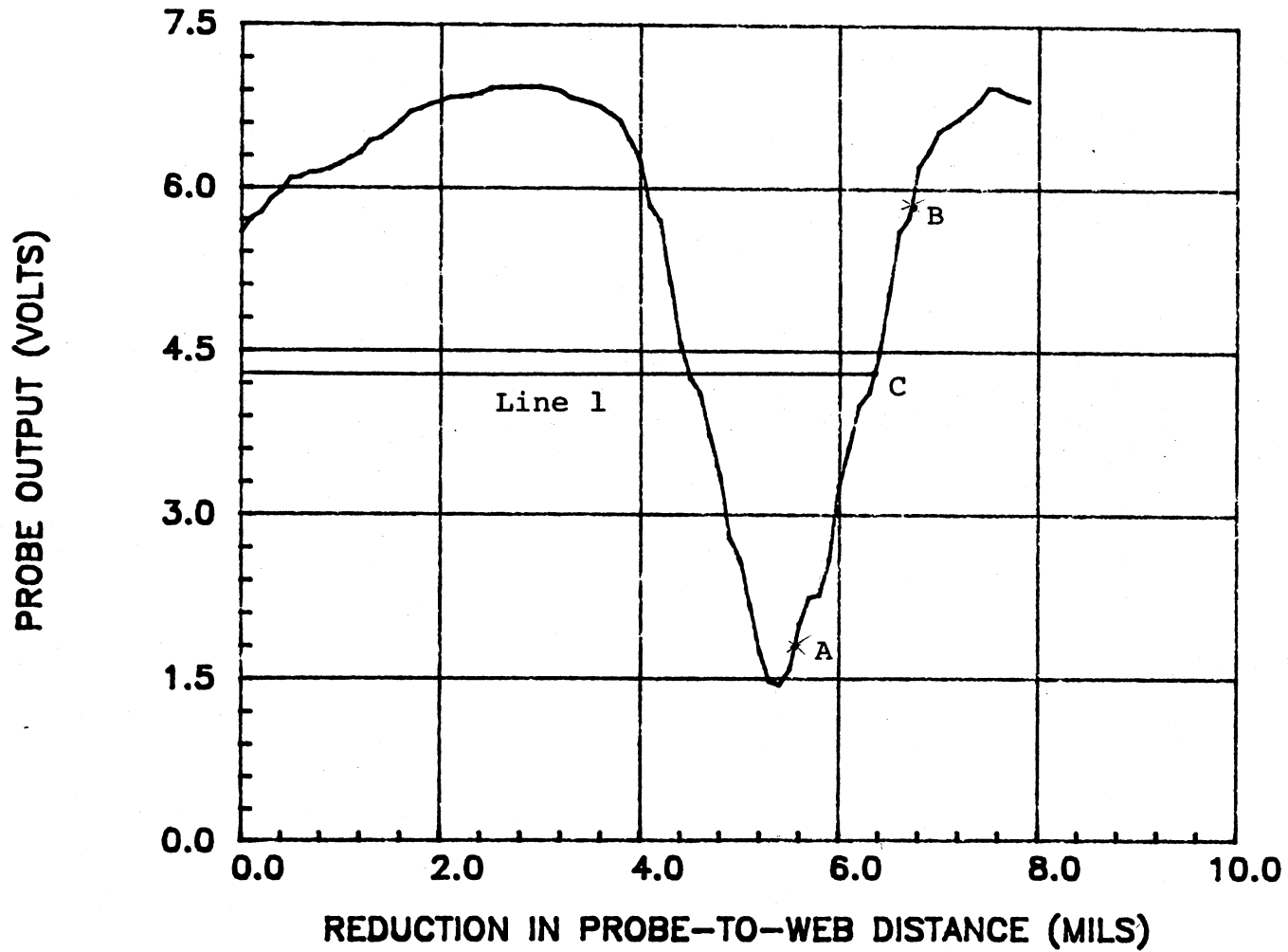


Figure 15. Typical Calibration Curve for  
White Polypropylene Web

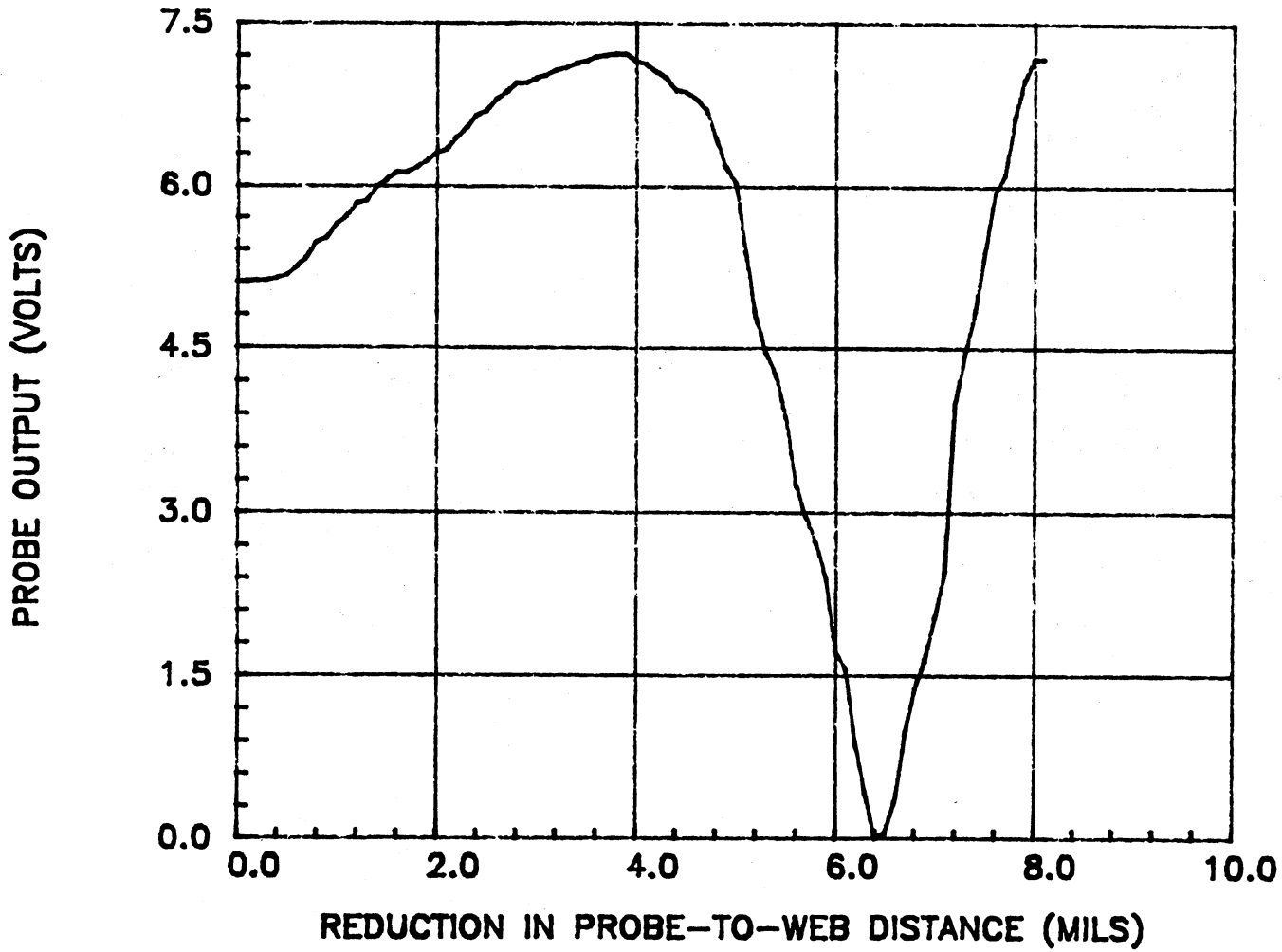


Figure 16. Typical Calibration Curve for Metallized Web

sensitive range for the measurements. Before measurements were taken, the probe was brought to a position where its output corresponds to point A on the calibration curve as shown in Figure 15. The web was then allowed to move at the desired speed and tension levels while the probe was looking perpendicularly at it as shown in Figure 14. The corresponding probe output will then be located on the calibration curve by drawing a straight line from probe output axis to a point on front slope between A and B (e.g. line 1 for a typical case), the difference of abscissa values of points A and C will correspond to the amount by which the web rises from the roller surface (i.e. the air gap thickness).

The rationale for the selection of the web materials used in this study will next be discussed.

#### 2.4 Selection Of Web Materials

Both the measurement technique and the test facility dictates the selection of the web material. On the one hand, the use of a Fotonic sensor requires that the web material should have a highly reflective surface. On the other hand, the use of a plexiglass roller demands that the web material should be electrically conductive in order to avoid the development of static charges which would degrade the measurements.

As mentioned earlier, webs of two different materials, a metallized (aluminum coated) and white

polypropylene (with anti-static coating) were used in all the reported experimental work. Both of these web materials were provided by Mobil Chemical Company, New York.

The metallized web was 0.0014 in. thick, while the white polypropylene web was 0.0017 in. thick. Both the webs were 6.0 in. wide. Further details concerning these web materials are provided in Appendix C.

## 2.5 Description Of Experiments

The experiments to be reported which employed the foregoing facilities and techniques involved the following tasks:

1. Measurement of air gap thickness in the region of uniformity for different line speeds and tension levels in the web.
2. Measurement of spatial variations in the air gap thickness along the width as well as along the wrap angle of the web.
3. Measurement of temporal variations in the air gap thickness along the width of the web.

The results of these measurements will be presented and discussed in the next chapter.

## CHAPTER III

### EXPERIMENTAL RESULTS

#### AND DISCUSSION

The first objective in this series of experiments was to experimentally measure the air film thickness between the moving flexible web and the supporting roller and to compare the experimental results to the air film thickness as predicted by the model of Tajuddin (1987). Of interest was the study of the effect of varying both the reduced tension and the web velocity on the resulting air film thickness in the uniformity region.

For the measurements to be reported, unless otherwise noted, the Fotonic sensor was positioned at the approximate geometrical center of the area of contact between the web and the roller (i.e.  $y/b=0$  and  $\phi=0^\circ$ ) with the fiber optic bundle perpendicular to the web surface.

Limitations of the experimental apparatus restricted static tensions to the range of 1.22  $lb_f/in$  to 2.11  $lb_f/in$ . The lower limit of static tension was just enough to avoid slippage between the web and the rubber drive roller while the upper limit was dictated by both the tension adjustment mechanism and the amount of tensile force which the web splice can withstand in order to



avoid web breakage. The upper limit on web velocity was approximately 254.5 in/sec (1272.5 fpm), dictated mainly by the output power of the drive motor of the web-moving machine, which for the present case was 1/3 hp. The practical lower limit on the velocity of the web was 50.0 in/sec (250 fpm), which was just enough to prevent the build-up of electro-static charges resulting from the physical contact of the inherently electrically non-conducting web and roller surfaces because of very thin entrained air film between the web and the roller at still lower velocities.

The experiments were performed by using both metallized and white polypropylene webs. The specifications as provided by the manufacturer of these web materials (Mobil Chemical Company), are presented in Appendix C. In all cases to be reported low coefficient of friction between the metallized web and the rubber drive roller restricted the experiments with the metallized web to be performed only at a tension level of 2.11 lb<sub>f</sub>/in. in order to avoid slippage at the rubber drive roller. The white polypropylene web was tested at two different static tension levels (i.e. at T=2.11 lb<sub>f</sub>/in and T=1.22 lb<sub>f</sub>/in). The computer programs used for storing and analyzing data on-line from the Fotonic sensor were developed during the course of this work and are presented and described in Appendix D.

The average uncertainty in the measurement of the

air film thickness was on the order of  $\pm 10\%$  at the web velocity of 50.0 in/sec (250 fpm), decreasing approximately to  $\pm 4\%$  at the web velocity of 254.5 in/sec (1272.5 fpm).

For the white polypropylene web, Figure 17 compares the experimentally measured and the theoretically predicted air gap thickness in the uniformity region for thirteen different web velocities at two different static tension levels. In these measurements, the probe was positioned at  $y/b=0$  along the width of the web and at  $\phi=0^\circ$  along the angle of wrap of the web. From this Figure, it can be observed that the experimental data in both cases, follow the same trend as predicted by theory but with a small positive offset. This small positive offset in the experimental data may possibly be attributed to the air film inertial effects which were not accommodated in the theoretical model. In order to verify this, it would be desirable to obtain additional measurements at higher line speeds which is not possible with the current facility. The effect of change in static tension can be seen from Figure 17, to be modelled correctly. Figure 17 shows that the air film thickness at any particular velocity increases as tension is reduced.

For the metallized web, Figure 18 compares the experimentally measured and the theoretically predicted air film thickness in the region of uniformity for thirteen different web velocities. Here also, the probe

*h = 15 mils = 0.5 x 10<sup>-3</sup> in.*  
*h x 10<sup>3</sup> = 0.5*  
*h = 0.5*

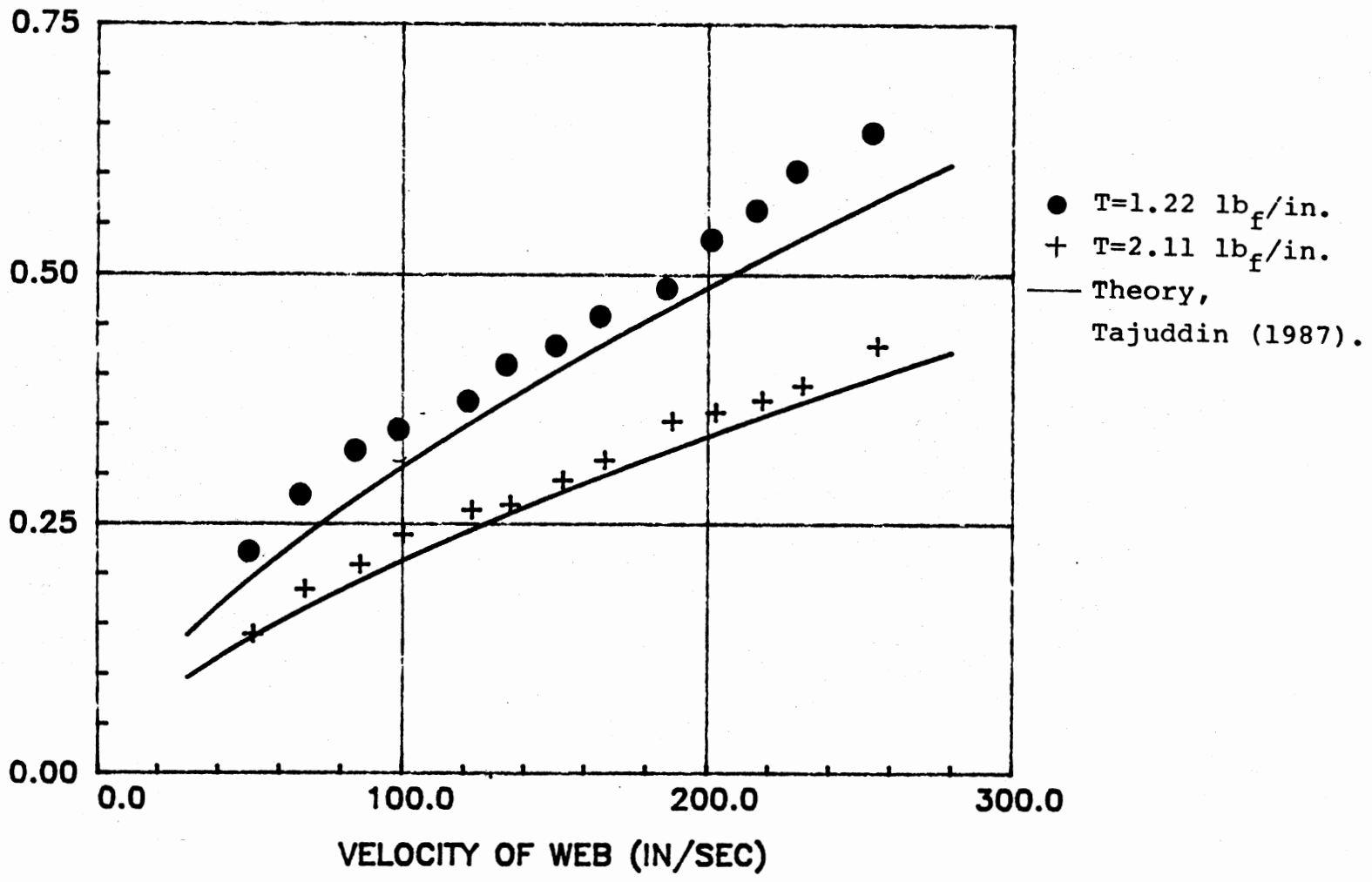


Figure 17. Effect of Velocity and Tension on Air Film Thickness in Constant Gap Region (White Polypropylene Web)

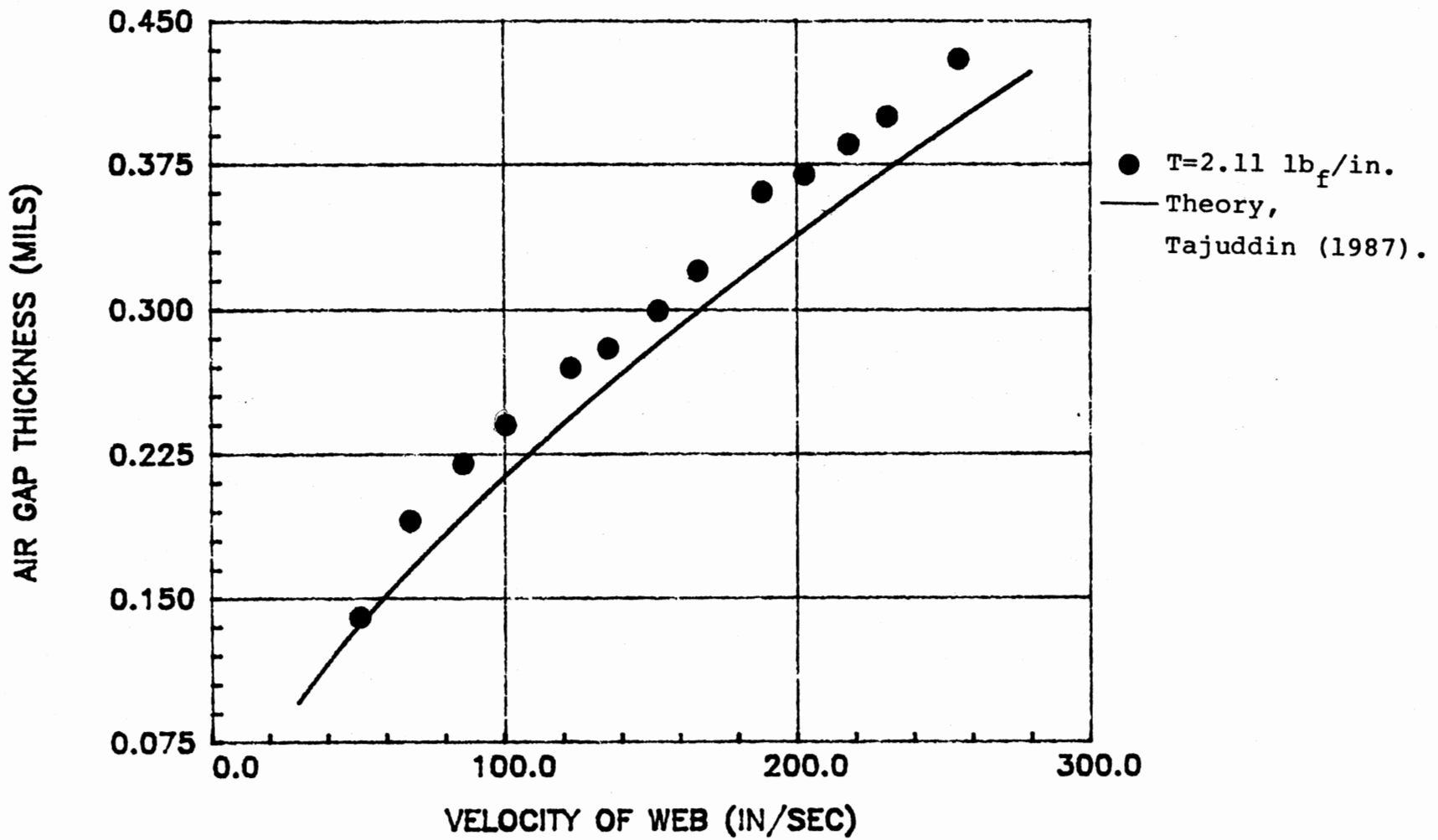


Figure 18. Effect of Velocity on Air Film Thickness in Constant Gap Region (Metallized Web)

was located at  $y/b=0$  and  $\phi=0^\circ$ . The experimental data is very similar to the previous case of the polypropylene web at the same static tension level. This suggests that there is not much effect introduced by the flexural and extensional rigidities (as presented in Appendix C) of these two web materials on the air film thickness in the current operating range of velocities and tension levels.

It can be concluded that the functional variation of the air film thickness  $h_0$ , agrees with theory i.e.,

$$h_0 \propto 0.643R(6\mu U/T)^{2/3} \quad (3.1)$$

In order to substantiate the functional relationship of equation (3.1), experimental data was curve fitted through the method of least squares. The curve fit shows that the exponent of equation (3.1) retains its value in all three cases while the constant of equation (3.1) changes as follows,

$$h_0=0.706R(6\mu U/T)^{2/3} \quad (3.2)$$

Figures 19 and 20 compares the experimental data with equation (3.2). Based on the above results and discussion, equation (3.2) is recommended for determining the air film thickness in constant gap region for all engineering calculations.

In order to investigate the azimuthal variation in the air film thickness in the uniformity region, measurements were made at different angular positions

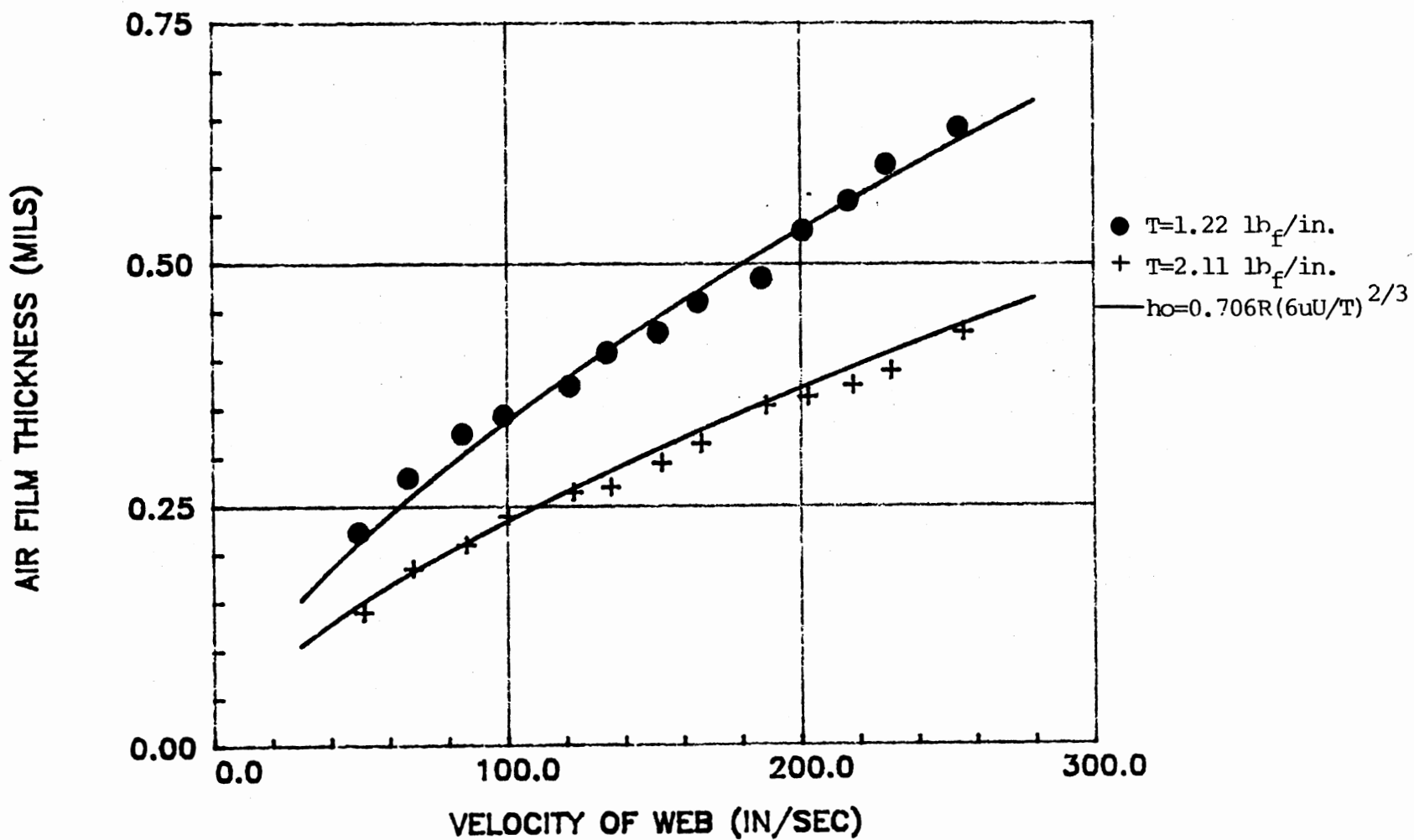


Figure 19. Curved Fitted Experimental Data  
(White Polypropylene Web)

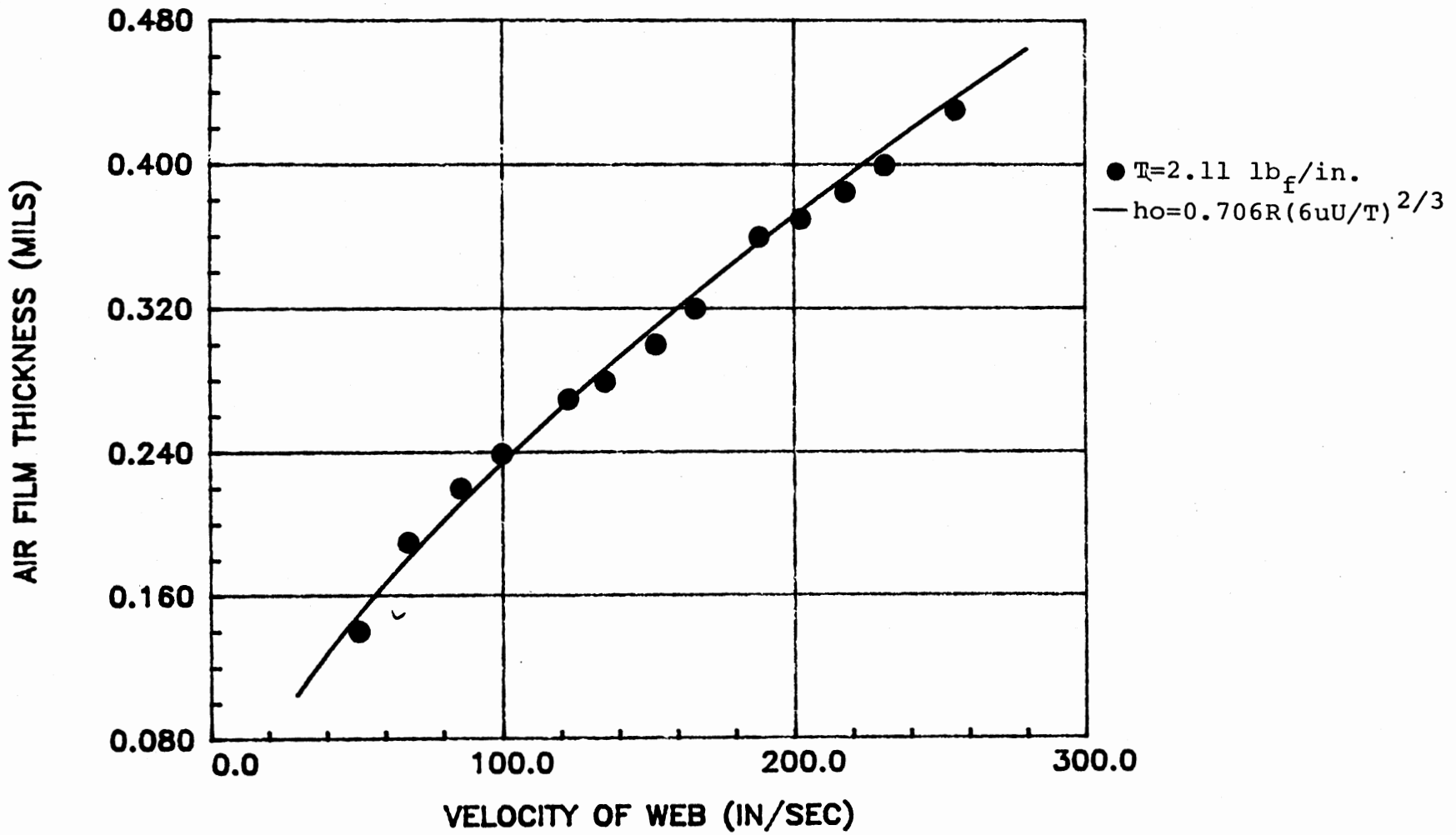


Figure 20. Curved Fitted Experimental Data  
 (Metallized Web)

i.e. at different  $\phi$  values, along the angle of wrap of the web i.e. along  $\beta$ . For this purpose, a slight modification was made in the basic test set-up in order to increase the total angle of wrap of the web i.e.  $\beta$  to 60 degrees (originally it was 20 degrees for the previously presented measurements). The modified set-up is shown in Figure 21. The probe was positioned at  $y/b=0$  for all measurements while its angular position was changed sequentially from  $\phi=0^\circ$  in 5 degree increments in both directions along the total angle of wrap of the web. Figure 22 shows the azimuthal variation in air film thickness for the case of a white polypropylene web moving with a velocity of 216.6 in/sec (1083 fpm) and at a static tension level of 1.22  $\text{lb}_f/\text{in}$ . Figure 22 shows that the air film thickness uniformity region exists only within central 70 percent of the statically determined total wrap angle. It is clear that a statically determined wrap angle and dynamic wrap angle are not the same. This decrease in wrap angle can be attributed to the presence of inlet and exit transitory regions in the dynamic case.

Figure 23 presents the azimuthal variation in air film thickness in the uniformity region for the metallized web, moving at a velocity of 254.5 in/sec (1272.5 fpm) with a static tension of 2.11  $\text{lb}_f/\text{in}$ . The data in Figure 23 follows approximately the same trend as the data in Figure 22 for white polypropylene web.





Figure 21. Modified Test Set-Up for High Wrap Angle ( $\beta=60^\circ$ )

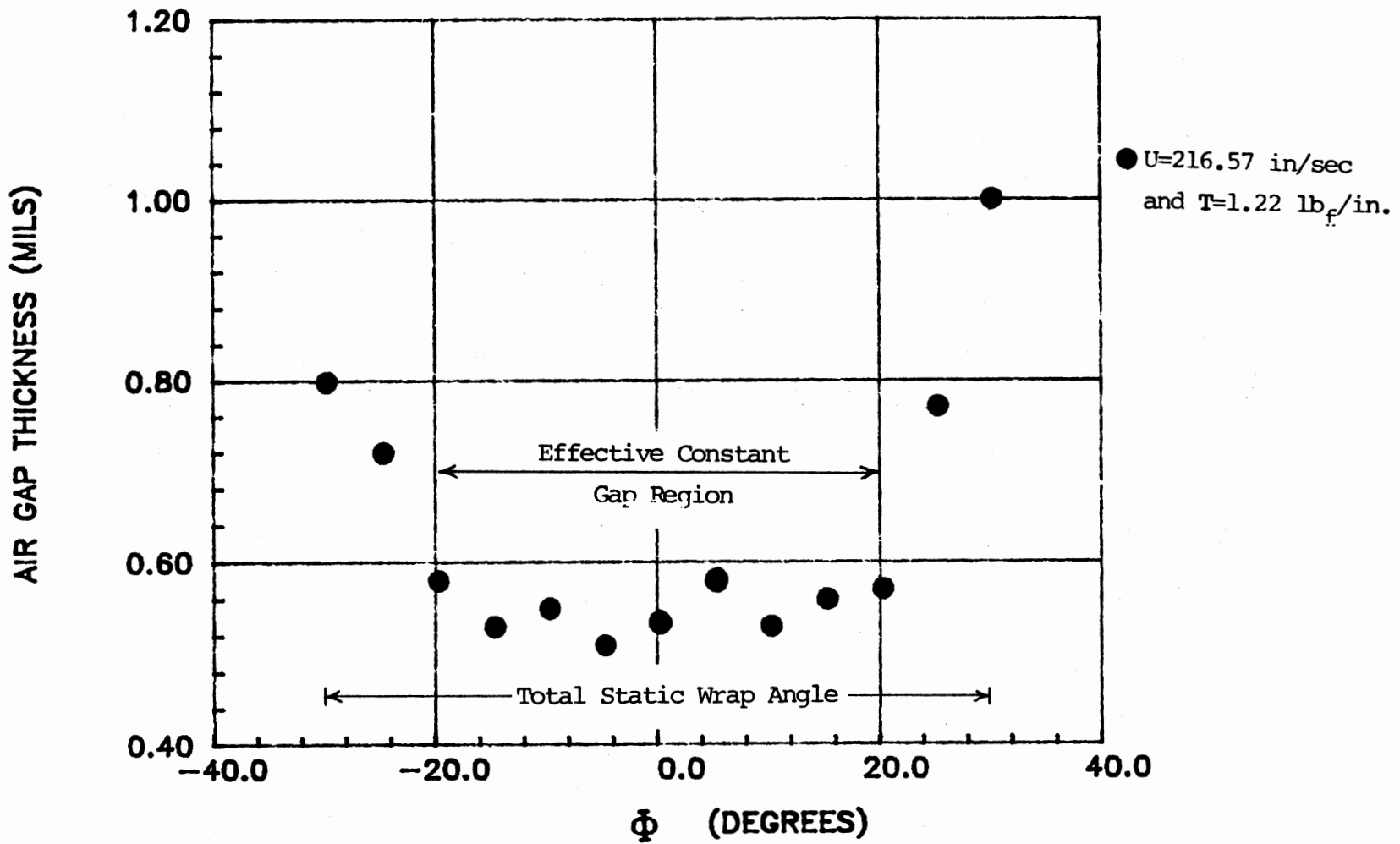


Figure 22. Azimuthal Variation in Air Film Thickness  
( $y/b=0.0$ , White Polypropylene Web)

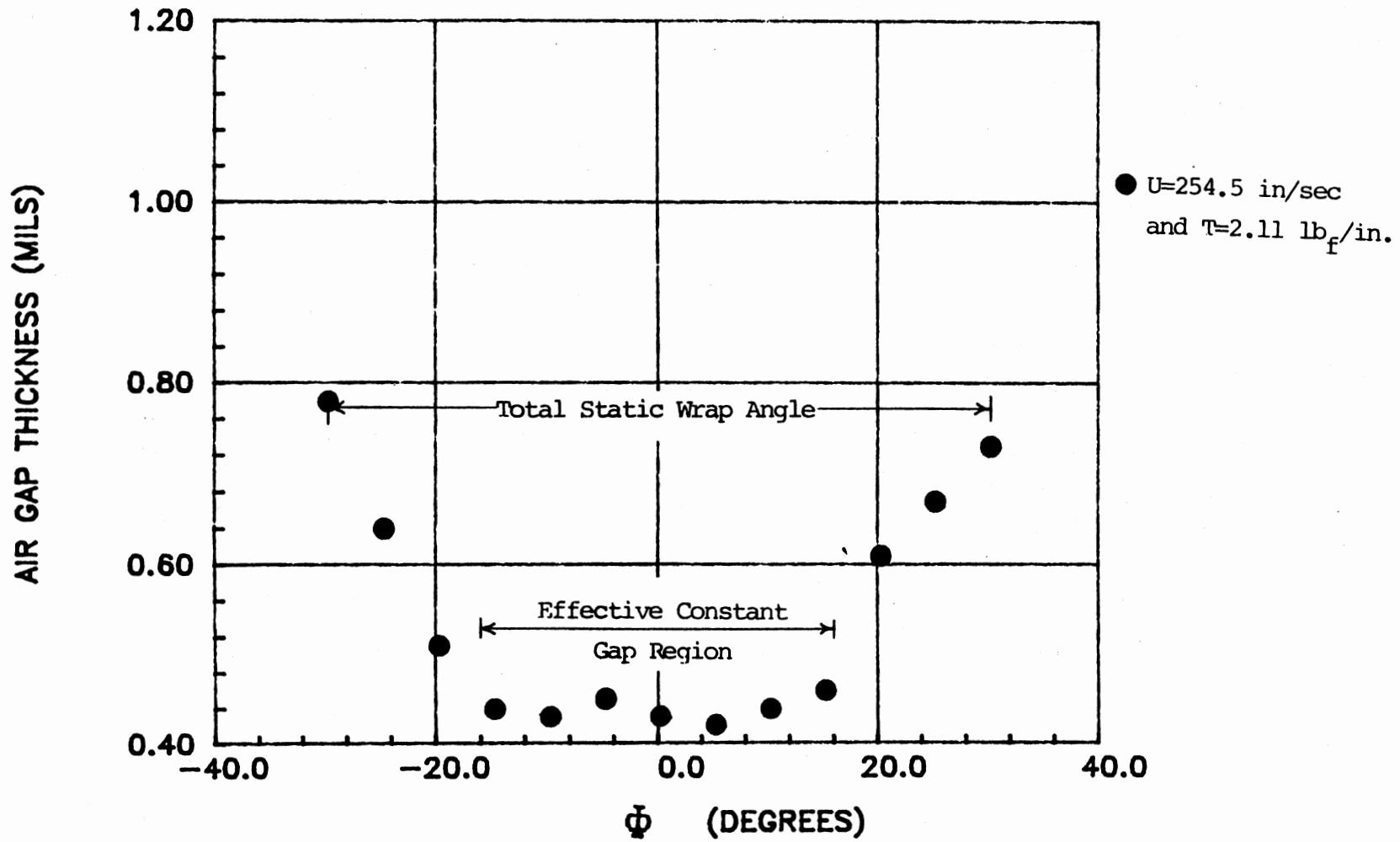


Figure 23. Azimuthal Variation in Air Film Thickness  
( $y/b=0.0$ , Metallized Web)

The theoretical model presented by Tajuddin (1987) assumes a web of infinite width while it is obvious that the real web has a finite width. A consequence of this is that side leakage of the entrained air may occur which implies that lateral non-uniformities in the air film thickness may exist. In order to investigate the effect of finite width (or the "edge effect") on the air film thickness in the uniformity region, measurements were made along the lateral extent of the web. The probe was positioned at  $\phi=0^\circ$  and was traversed in increments of  $y/b=0.1666$  which corresponds to steps of 0.5 inch in the range  $(-0.66 \leq y/b \leq 0.66)$  and in increments of  $y/b=0.0833$  which corresponds to steps of 0.25 inches in the ranges of  $(-0.9166 \leq y/b < -0.66)$  on one side and  $(0.66 < y/b \leq 0.9166)$  on the other side along the width of the web. Figure 24 shows the lateral variation in air film thickness in the uniformity region for the metallized web, moving with a velocity of 254.5 in/sec (1272.5 fpm) and static tension level of 2.11 lb<sub>f</sub>/in. This plot shows that the air film thickness is reduced sharply towards the outer edges of the web. From Figure 24 it can be observed that for the present case a uniformity region exists only for approximately the central 50 percent (i.e.  $-0.5 \leq y/b \leq 0.5$ ) of the total width of the web. This reduction in air film thickness towards the edges of the web is attributable to leakage of the air from the edges. This can be understood by

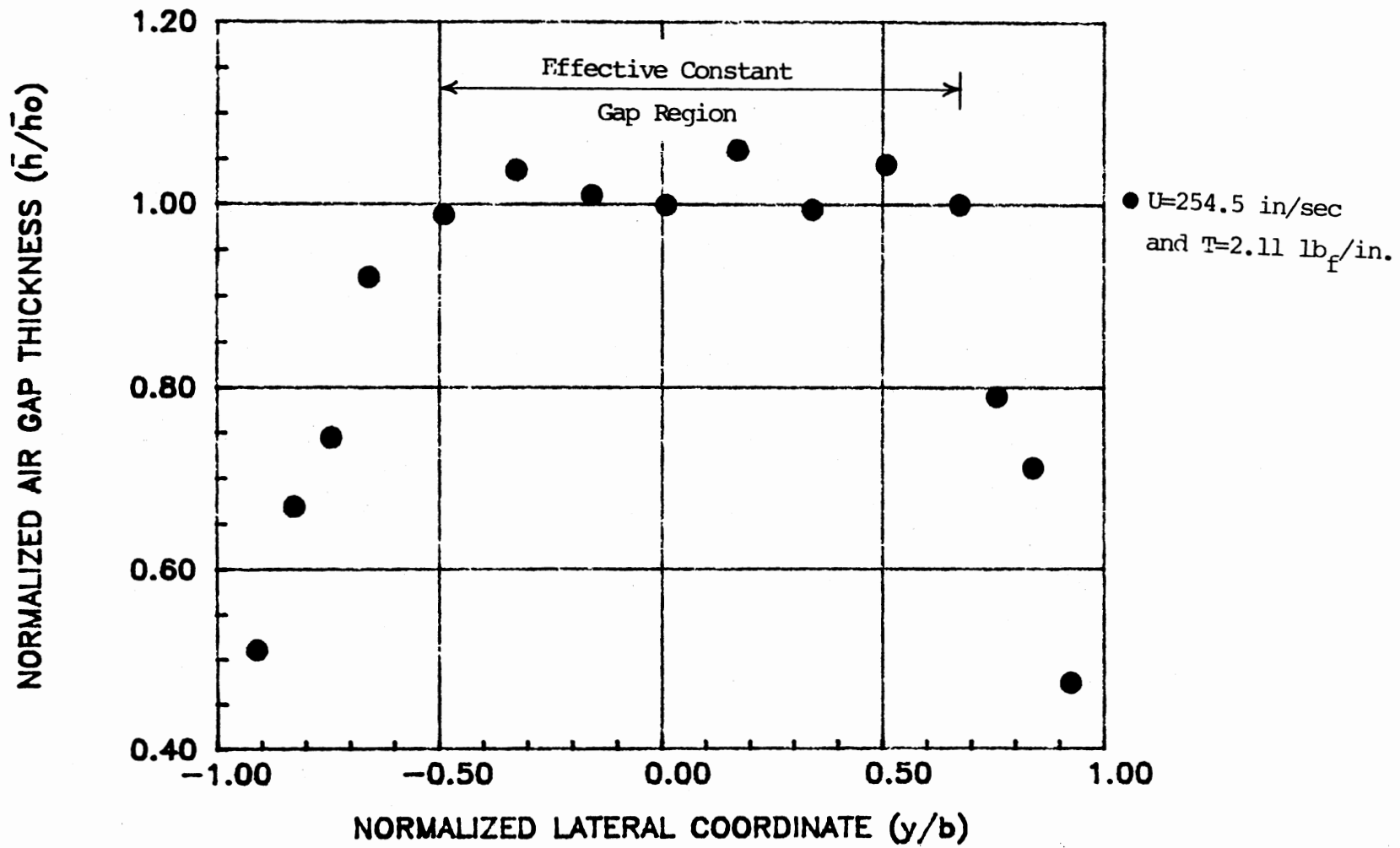


Figure 24. Lateral Variation in Air Film Thickness  
( $\phi=0^\circ$ , Metallized Web)

applying a 1-D Reynold's lubrication equation for the flow of air in the Y-direction (i.e. along the width of the web). The pressure decreases from the pressure in uniformity region to ambient pressure along the outer edges of the web and thus causes a negative pressure gradient  $dP/dY$  and according to Reynold's lubrication equation this can occur only if  $h < h_0$ , which corresponds to decrease in air film thickness towards the outer edges.

Figure 25 presents the lateral variation in air film thickness with white polypropylene web moving at a velocity of 254.5 in/sec (1272.5 fpm) and a static tension of 2.11  $lb_f/in$ . These data points also shows that the effective uniformity region lies in the range  $-0.5 \leq y/b \leq 0.5$  (i.e. central 50 percent of the total width of the web).

An interesting feature of the data in Figure 25 is that it is not perfectly symmetrical with respect to the center of the web (i.e. w.r.t  $y/b=0$  and  $\phi=0^\circ$ ). It can be seen that air gap starts reducing relatively close to the center (i.e.  $y/b=0$ ) along the width of the web in the range specified by  $(-1 < y/b < 0)$  than in the range  $(0 < y/b < 1)$ . One reason for this might be the presence of circumferential groove-like wear marks in that particular range on the roller surface which were allowing more air to escape from these grooves and thus resulting in reduced air gap thicknesses. This explanation is partly

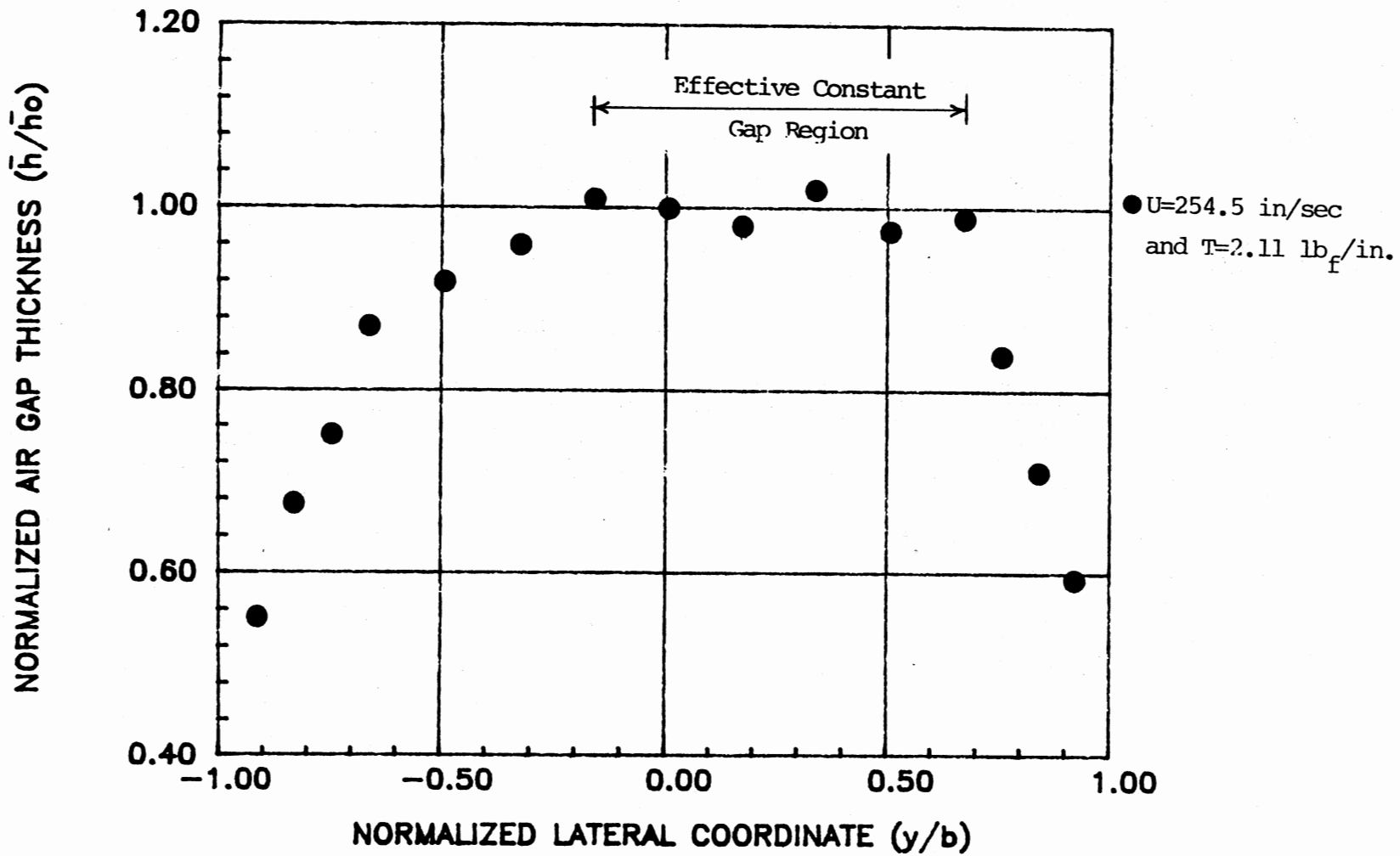


Figure 25. Lateral Variation in Air Film Thickness ( $\phi=0^\circ$ , White Polypropylene Web)

supported by Figure 26, where the same readings were taken for that particular half of the roller, by pivoting the roller 180 degrees about its axis so that the range  $(-1 \leq y/b \leq 0)$  in Figure 26 corresponds to the range  $(1 \leq y/b \leq 0)$  in Figure 25.

Also referring back to Figure 24 which represents the lateral variation in the air film thickness with metallized web, it can be seen here that there is no preferred direction for the reduction in the air film thickness because the surface of the roller in contact with the web did not have any wear marks when these tests were run. The data is almost symmetrical with respect to the center of the web (i.e.  $y/b=0$ ) and the effective uniformity region lies in the range  $-0.5 \leq y/b \leq 0.5$  (i.e. central 50 percent of the total width of the web).

Figure 27 shows a photograph of the metallized web which had been used for more than 100 runs. The most noticeable aspect of Figure 27 is the removal of the metal coating from the web surface near the outer edge due to increased contact with the stationary roller as a result of the loss of the air film near the edge as suggested in Figures 24, 25, and 26 in the region close to the outer edges of the web.

The mathematical formulation of the effect of finite width (the "edge effect") can be obtained from a "first principles" approach. The prediction of the lateral foil topography or the lateral air film thickness, requires a



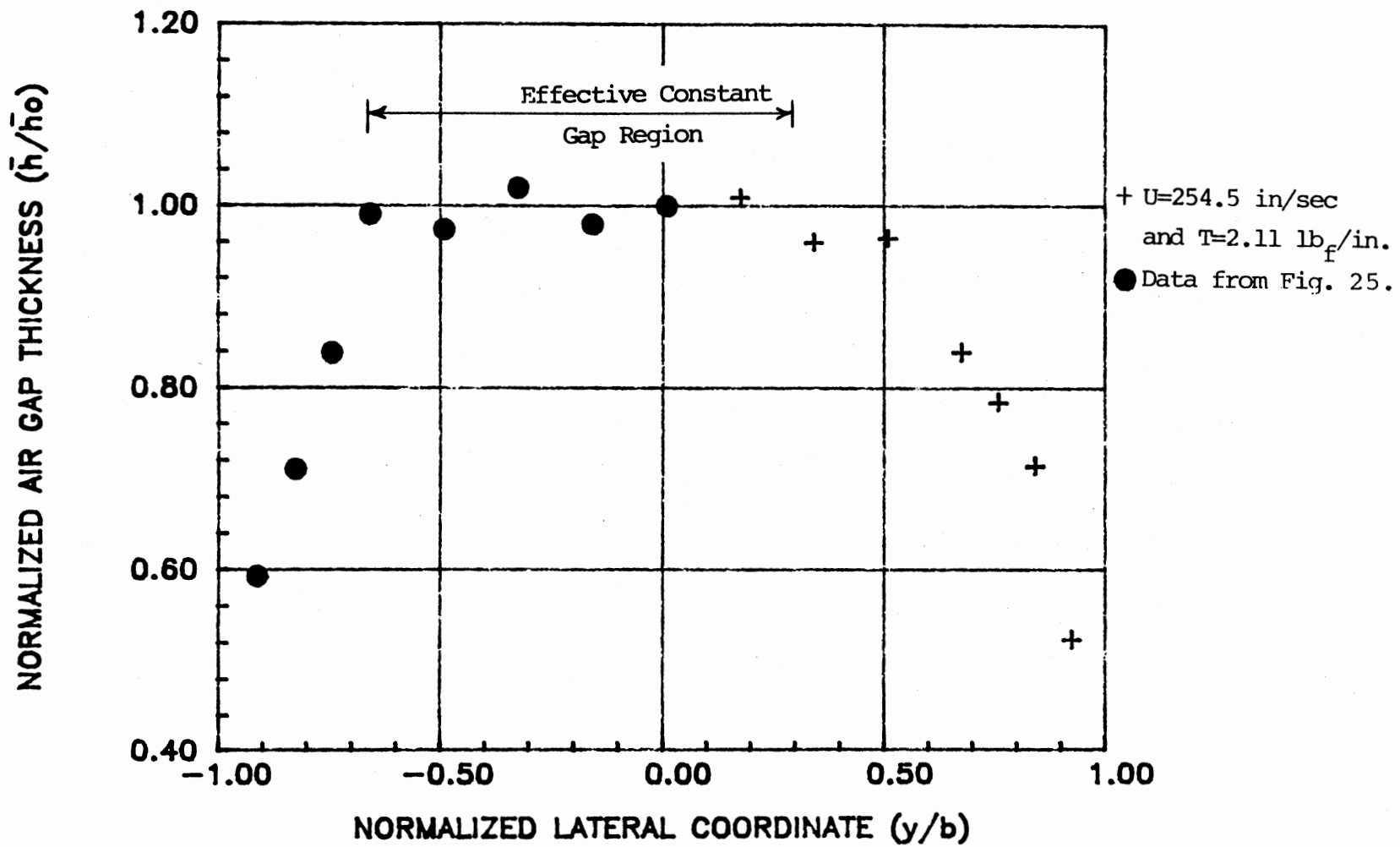


Figure 26. Effect of Grooved Roller Surface on Air Film Thickness

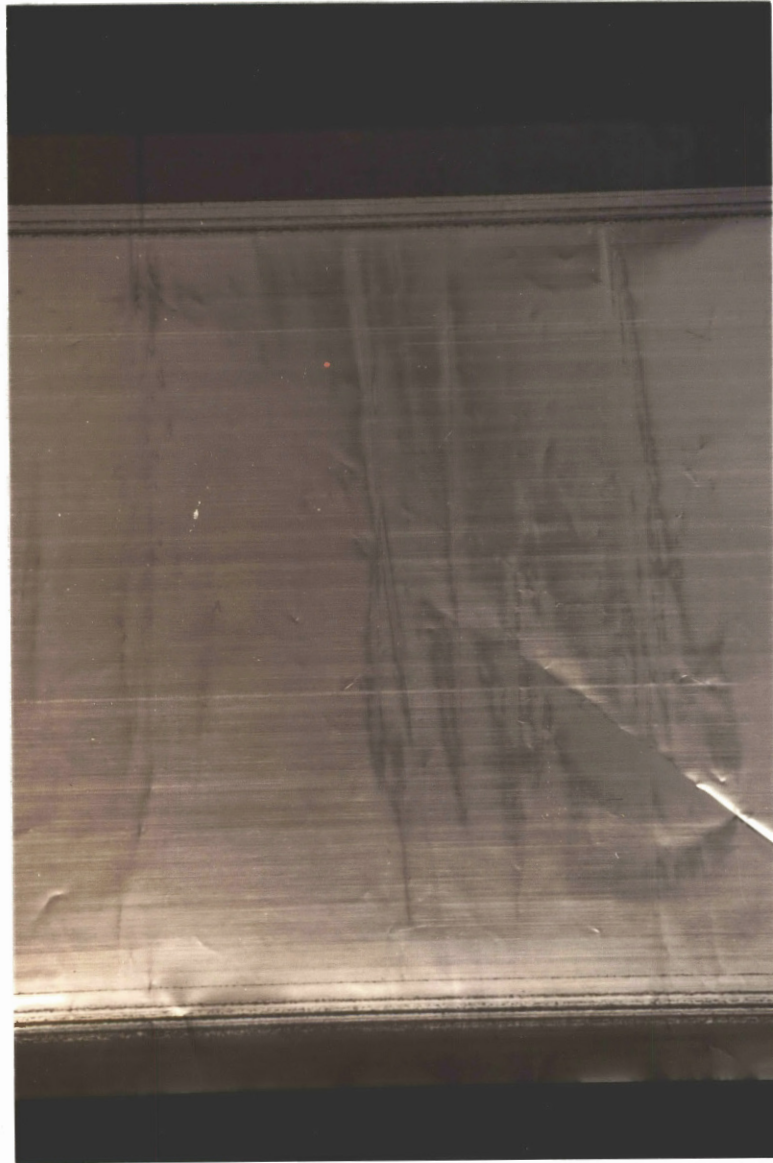


Figure 27. View of Worn-Edge Metallized Web

simultaneous solution of equations concerning the hydrodynamics of the air film and the web equilibrium dynamics.

Figure 28 shows respectively the schematic of the basic geometric configuration of the problem and the coordinate system that will be used for the mathematical formulation. For the analysis, it is assumed that a web of thickness  $t$  and width  $2b$  passes over a stationary roller of radius  $R$  with a uniform velocity of  $U_w$  under a uniform tension of  $T$ .

Regarding the general hydrodynamic equation, it is assumed that a one dimensional i.e.  $y$ -directed, flow with a pseudo-parabolic variation in velocity across the air gap thickness (i.e. in the  $Z$ -direction in order to satisfy no slip conditions at the top and bottom surfaces), to which the Navier-Stoke's equation can be applied as the basic hydrodynamic equation. For the present case, flow is steady and gravity effects are negligible. The application of Navier-Stoke's equations will yield, between location 1 (i.e. at  $y/b=0$ ) and location 2 ( i.e. at  $0 < y/b \leq 1$ ) which is any downstream position along the half width of the web, as shown in Figure 28 and further assuming that at  $y/b=0$  flow starts developing (i.e the bulge in velocity profile is very small at  $y/b=0$  and increases as  $y/b$  increases),

$$u \frac{\partial v}{\partial x} + v \frac{\partial v}{\partial y} + w \frac{\partial v}{\partial z} = -\frac{1}{\rho} \frac{\partial P}{\partial y} + \nu \left[ \frac{\partial^2 v}{\partial x^2} + \frac{\partial^2 v}{\partial y^2} + \frac{\partial^2 v}{\partial z^2} \right] \quad (3.3)$$

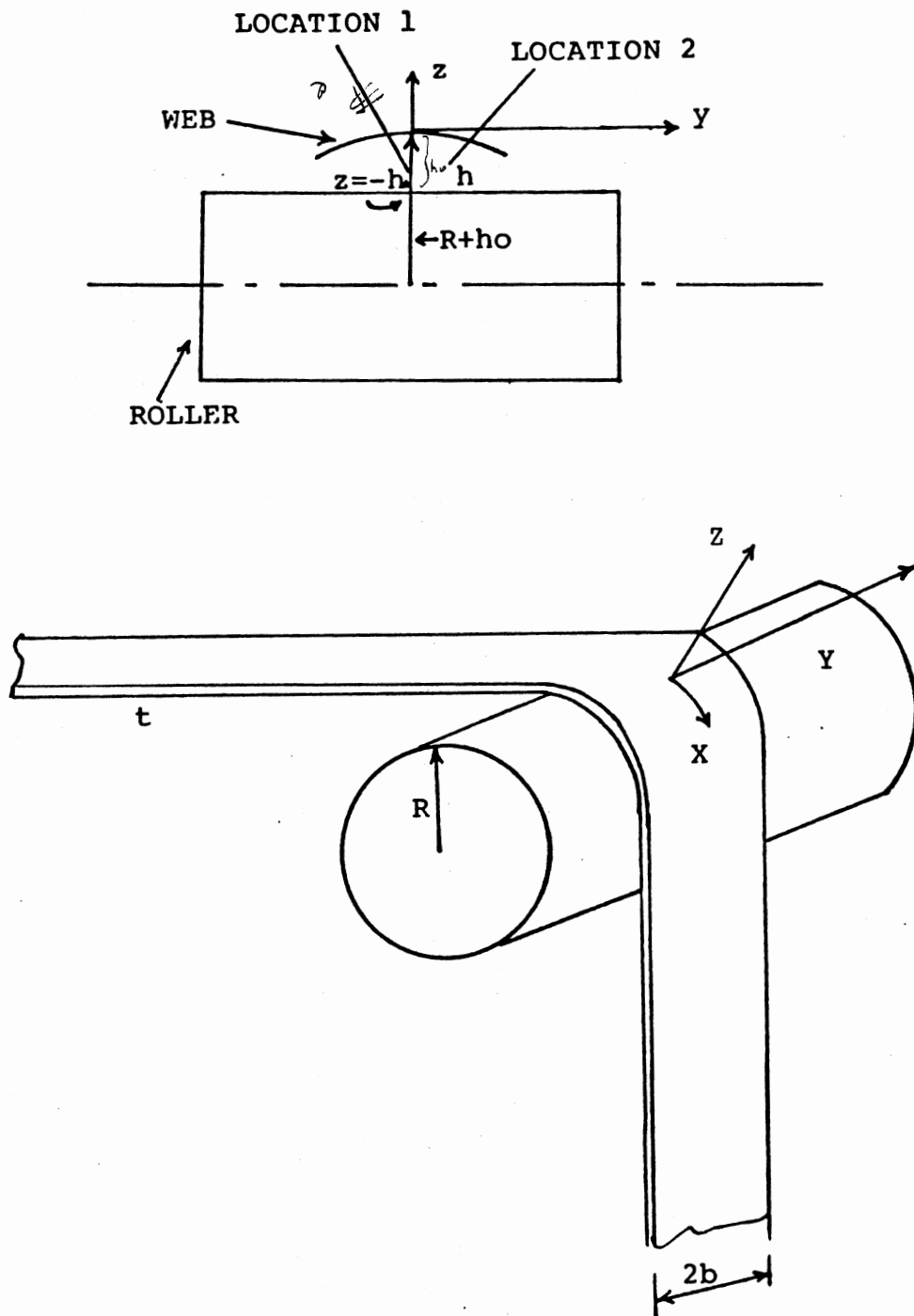


Figure 28. Schematic of Finite Width Effect

$$\partial P / \partial x = \partial P / \partial z \approx 0 \quad (3.4)$$

and the continuity equation will be given by,

$$\partial u / \partial x + \partial v / \partial y + \partial w / \partial z = 0 \quad (3.5)$$

after incorporating the assumptions, equation (3.3) and (3.5) become respectively,

$$\partial P / \partial y = \mu [ \partial^2 v / \partial y^2 + \partial^2 v / \partial z^2 ] \quad (3.6)$$

$$\partial v / \partial y = 0 \quad (3.7)$$

Regarding the web equilibrium dynamics, the equilibrium equation of the web relates the displacement of the web surface from the cylinder subtended by the web at  $r=R+h_0$  (as shown in Figure 28), to the tension in the web.

We assume that a thin cylindrical web of arc length  $s$ , is bent along the edges and whose deflections from the circular cylindrical shape are of the same order as the thickness. Under these assumptions we can use the plane-stress approximations to the linearized equations of elasticity. Thus the equilibrium equation will be given by,

$$(EI/s) \, d^4 z / dy^4 = T_0/R - (P-P_a) \quad (3.8)$$

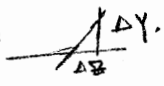
Where  $z$ , is the deviation of the web surface from the cylinder  $r=R+h_0$ ,  $P_a$  is the atmospheric pressure,  $P$  is

the pressure in the entrapped air film,  $T_0$  is the applied tension,  $E$  is the modulus of elasticity.  $I$ , the moment of inertia for the shell of thickness  $t$  and radius  $R_1$  is given by,

$$I = \frac{0.1098(R_1^4 - r^4) - 0.283R_1^2r^2(R_1 - r)}{R_1 + r} \quad (3.9)$$

When the ratio  $t/R_1$  is very small, the inertia is given by,

$$I \approx 0.3tR_1^3 \quad (3.10)$$

The prerequisite for applying equation (3.8) is an approximation which demands that  $(dz/dy)^2$  shall be slop everywhere negligible compared with unity and for the  case under study this condition is always true.

The governing equation which can relate the displacement of the web 'z' with the lateral coordinate 'y' can be derived as follows:

1. First assuming a lateral (y) variation in the center line velocity  $V_{MAX}$ , which is approximated by a 5<sup>th</sup> order polynomial, and then evaluating the constants with the help of following boundary conditions for the geometry of Figure 29,

a.	$V_{MAX}=0$	at	$y=0$	}	(3.11)
b.	$V_{MAX}'=0$	at	$y=0$		
c.	$V_{MAX}=V_{\infty}$	at	$y=b$		
d.	$V_{MAX}=-V_{\infty}$	at	$y=-b$		

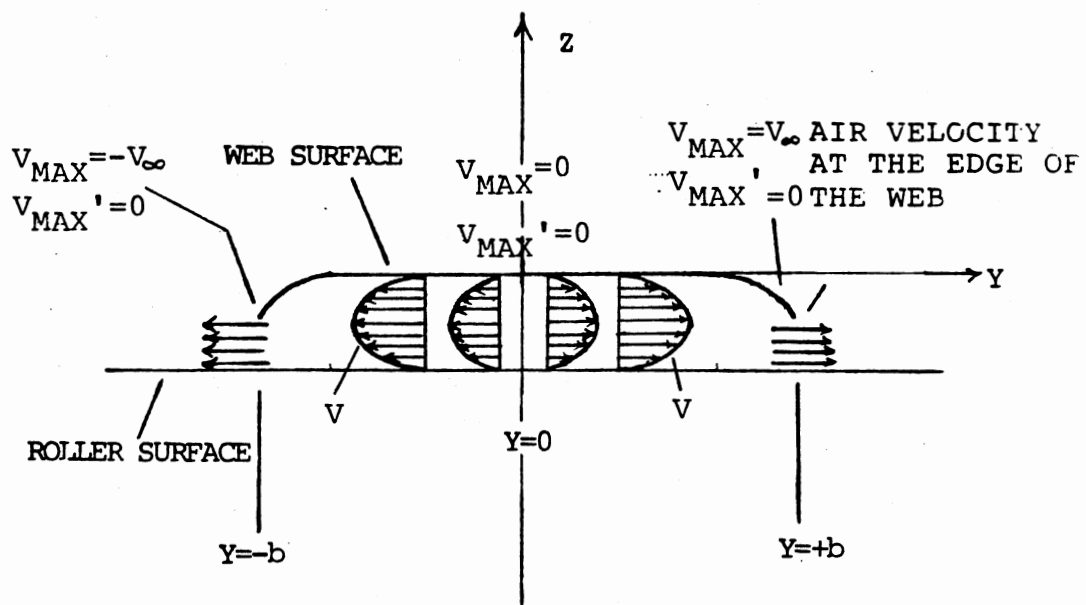


Figure 29. Lateral Flow Along with Imposed Boundary Conditions

$$e. \quad V_{MAX}'=0 \quad \text{at} \quad y=\pm b$$

The lateral resulting velocity variation is given by,

$$V_{MAX} = 2.5V_{\infty}(y/b)^3 - 1.5V_{\infty}(y/b)^5 \quad (3.12)$$

where ' $V_{\infty}$ ' is the velocity at which air leaks from the constant gap region at the edge of the web and 'b' is the half width of the web. Figure 30 shows the normalized center line velocity variation i.e.  $V_{MAX}/V_{\infty}$  distribution along the width of the web.

2. The combined velocity variation 'v' after incorporating the pseudo-parabolic variation along the air gap thickness is given by,

$$v(y,z) = -4 * V_{MAX}(y) * [ z/h + (z/h)^2 ] \quad (3.13)$$

2. Substituting  $V_{MAX}$  from equation (3.12) to equation (3.13) and then double differentiating the resulting equation w.r.t y and z separately.

3. Substituting the double derivatives of velocity in equation (3.6) and then integrating the resulting pressure term at the center line (i.e at  $z=h_0/2$ ) along the half width because of the symmetrical nature of the problem. We obtain,

$$P(y) = P_{c.g} - T_0 h_0^2 / 3Rb * S \quad (3.14)$$

where S is given by,



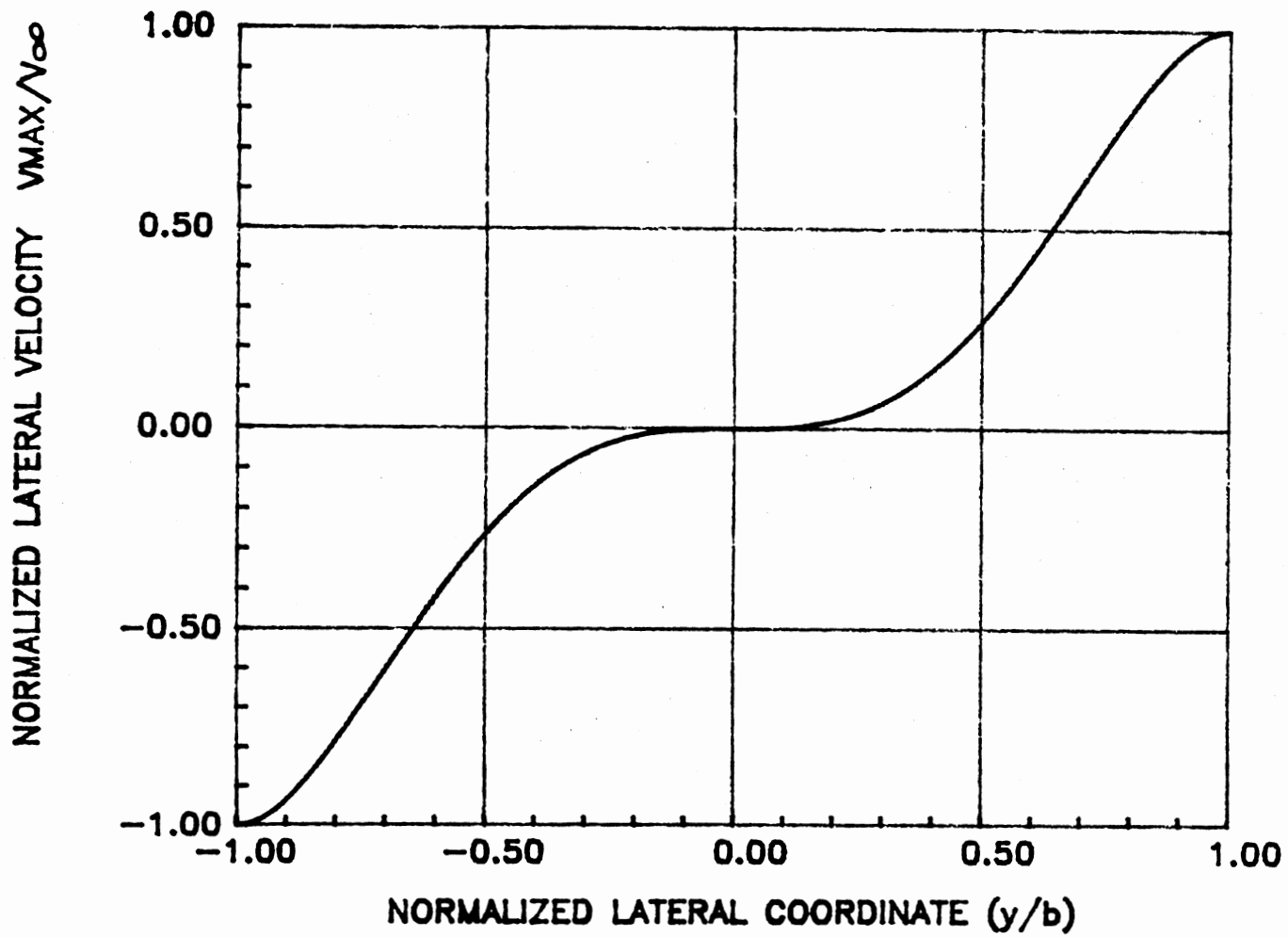


Figure 30. Velocity Variation Along the Width of the Web

$$S = (5/h_0^2 b^3 y^4 - 2/h_0^2 b^5 y^6 - 15/2b^3 y^2 + 15/2b^5 y^4) \quad (3.15)$$

Figure 31 shows the normalized theoretical pressure distribution along the width of the web.

4. Then substituting the pressure 'P' from equation (3.14) to equation (3.8), the resulting equation will be as follows,

$$d^4 z/dy^4 = (T_0 \beta h_0^2 / 0.9 E t R^3 b) * S \quad (3.16)$$

The following boundary conditions are used to solve the above governing equation,

$$a. \quad d^3 z/dy^3 = 0 \quad \text{at} \quad y = 0 \quad (3.17)$$

i.e. the transverse shear stress will be zero at the center of the web width.

$$b. \quad d^2 z/dy^2 = 0 \quad \text{at} \quad y = \pm b \quad (3.18)$$

i.e. the anticlastic curvature will be zero at the two outer edges.

$$c. \quad dz/dy = 0 \quad \text{at} \quad y = 0 \quad (3.19)$$

$$d. \quad z = 0 \quad \text{at} \quad y = 0$$

i.e. the conditions resulting from the symmetry about the center of the web width. The complete solution of the equation (3.16) is given by,

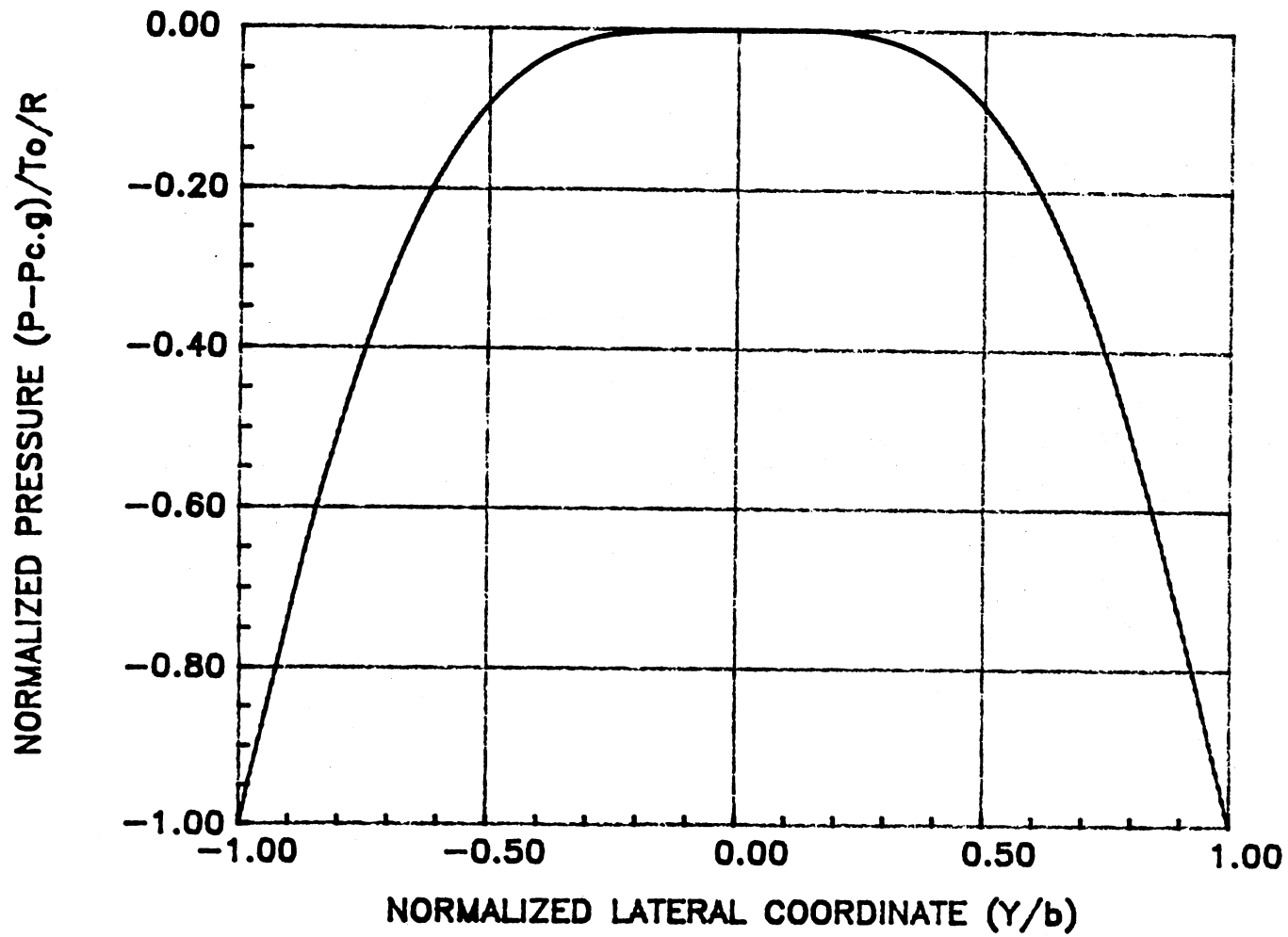


Figure 31. Pressure Variation Along the Width of the Web

$$z = (T_0 h_0^2 \beta / 0.9 E t R^3 b) * [ A y^8 - B y^{10} - C y^6 + D y^8 ] - E y^2 \quad (3.20)$$

where,

$$\begin{aligned} A &= 2.976 * 10^{-3} * b^{-3} * h_0^{-2} \\ B &= 3.9682 * 10^{-4} * b^{-5} * h_0^{-2} \\ C &= 2.08 * 10^{-2} * b^{-3} \\ D &= 4.46428 * 10^{-3} * b^{-5} \\ E &= 9.8001 * 10^{-6} \end{aligned} \quad (3.21)$$

Comparison of Experimental Data With Theoretical Model:  
 Figures 32 compares the experimental data of lateral air gap variation for the white polypropylene web with the theory i.e. equation (3.20). It can be seen here that all along the width of the web experimental data is in good agreement with the theoretically predicted values except at the outer edges. This may be because of the presence of very thin wear marks which were causing more air to leak out and equation (3.20) does not incorporate such effects, or due to experimental errors.

Figure 33 compares the experimental data with the theoretically predicted values for the case of metallized web.

The mathematical model predicts that the air film thickness in the uniformity region remains constant at some nominal value for a given set of operating conditions but in fact the temporal fluctuations in the air film thickness is always present which makes the web

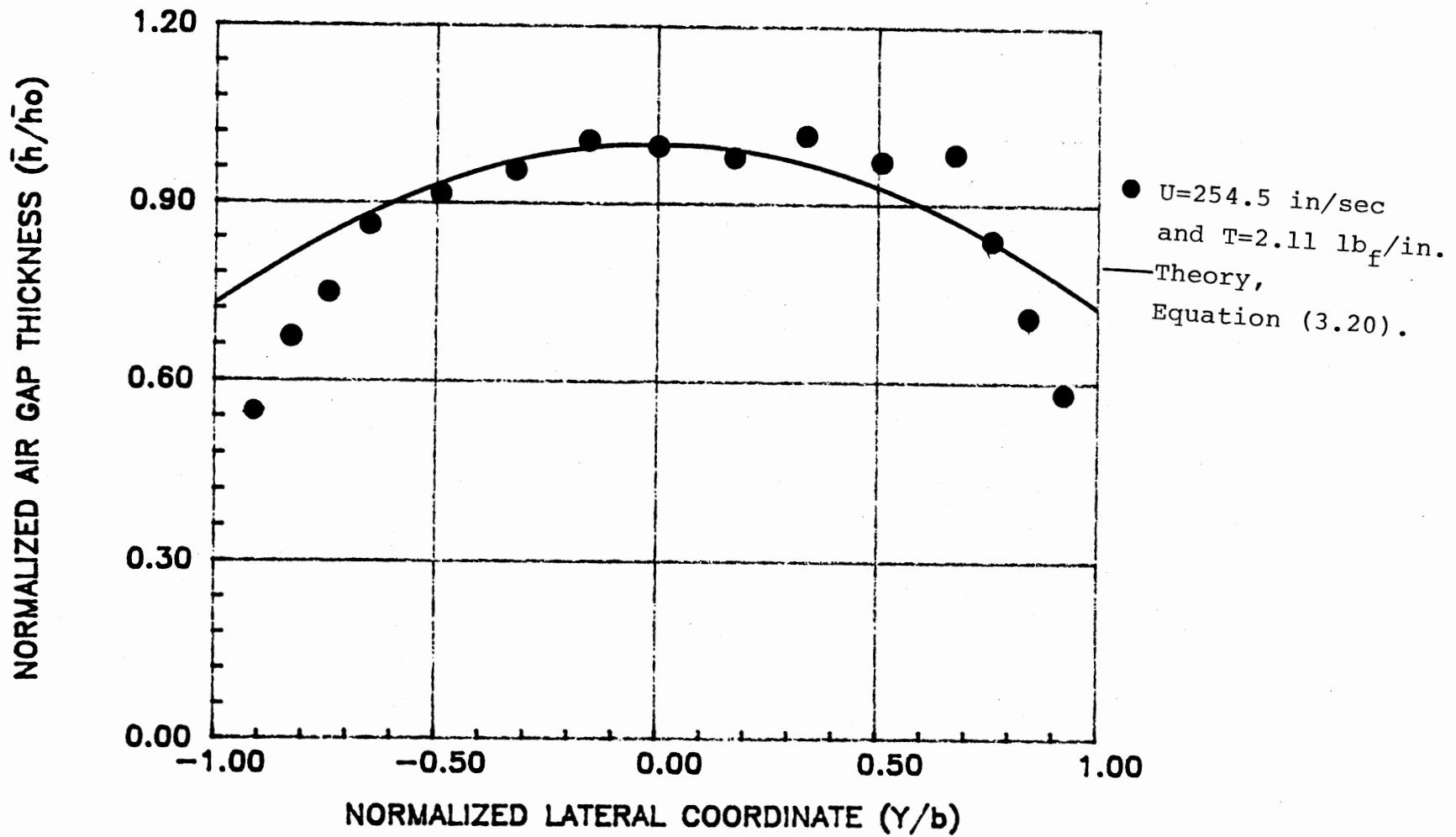


Figure 32. Comparison of Experimental Data with Equation (3.20) (White Polypropylene Web)

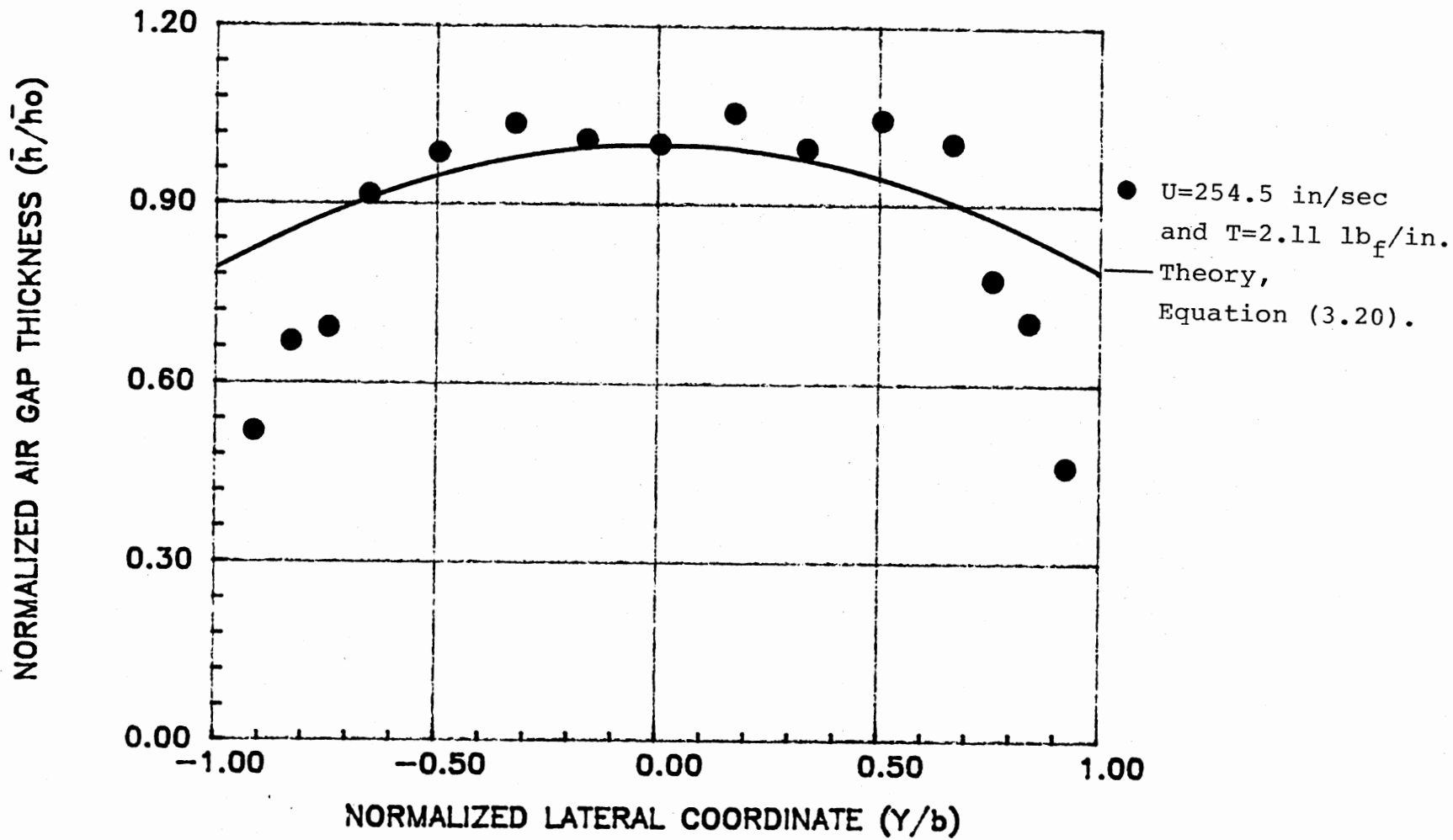


Figure 33. Comparison of Experimental Data with Equation (3.20) (Metallized Web)

fluctuate around some nominal value. To investigate the rms fluctuation of the air film thickness, measurements of the air film thickness were made along the lateral extent of the web. The probe was positioned at  $\phi=0^\circ$  and traversed in increments of  $y/b=0.1666$  which corresponds to steps of 0.5 inch in the range  $(-0.833 \leq y/b \leq 0.833)$  along the width of the web.

Figure 34 shows the lateral rms fluctuation of the air film thickness in the uniformity region for the metallized web, moving with a velocity of 254.5 in/sec (1272.5 fpm) and a static tension of 2.11 lb<sub>f</sub>/in. The ordinate on this plot is the ratio of the rms value of the difference between the instantaneous local air gap thickness and the mean local air gap thickness to the mean air gap thickness at  $y/b=0$  (i.e. at the center of the web width). This plot shows that the rms fluctuation of the air film thickness is much higher towards the edges than at the center of the web. The photograph of metallized web as presented in Figure 27 when studied in reference to this plot tells that the web's outer edges were touching the roller surface more frequently than the center of the web and hence the removal of metal coating.

Figure 35 shows the lateral variation in rms fluctuation of the air film thickness for the white polypropylene web, moving at a velocity of 254.5 in/sec (1272.5 fpm) with a static tension of 2.11 lb<sub>f</sub>/in. The data in Figure 35 follows approximately the same trend as

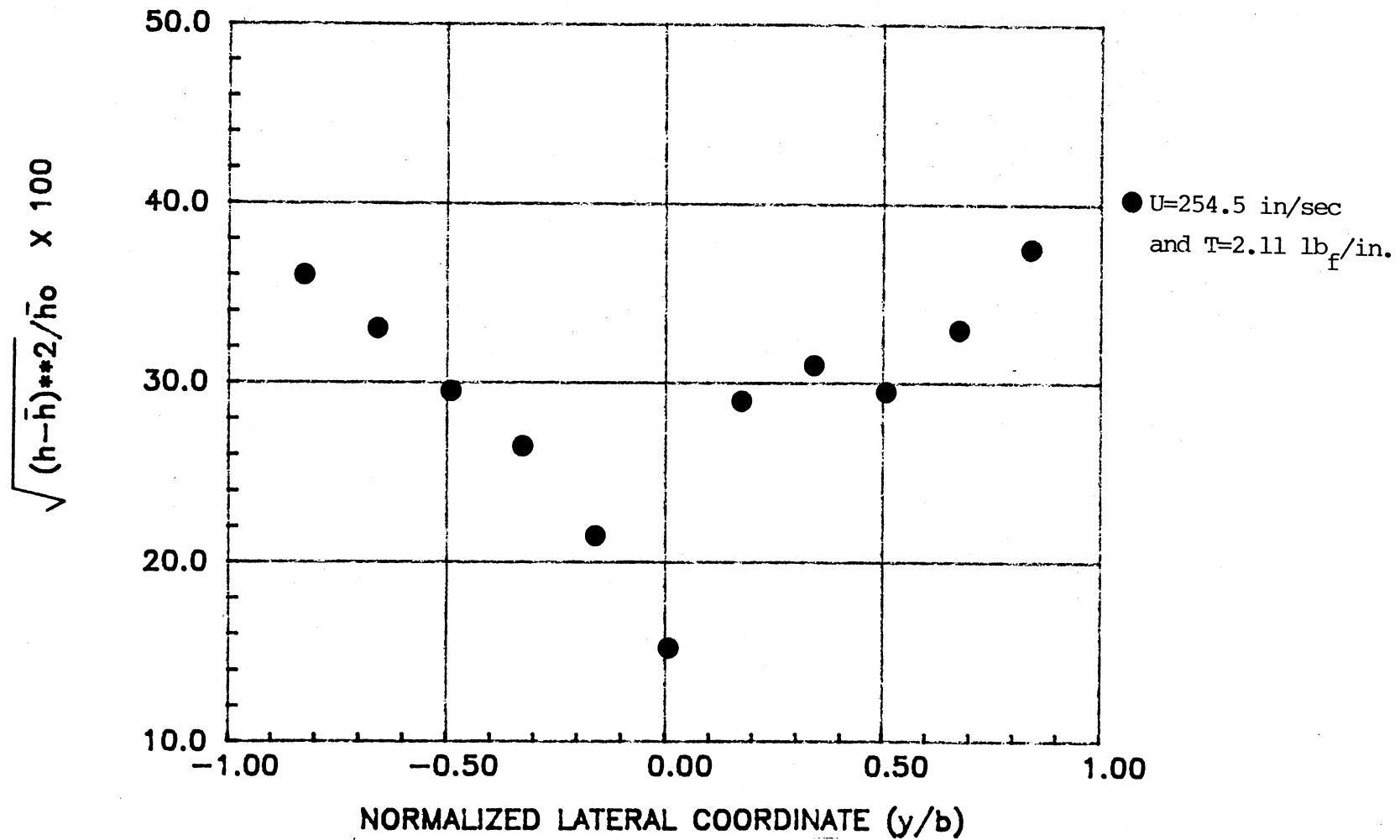


Figure 34. Lateral RMS Fluctuation of Air Film Thickness in Constant Gap Region (Metallized Web)



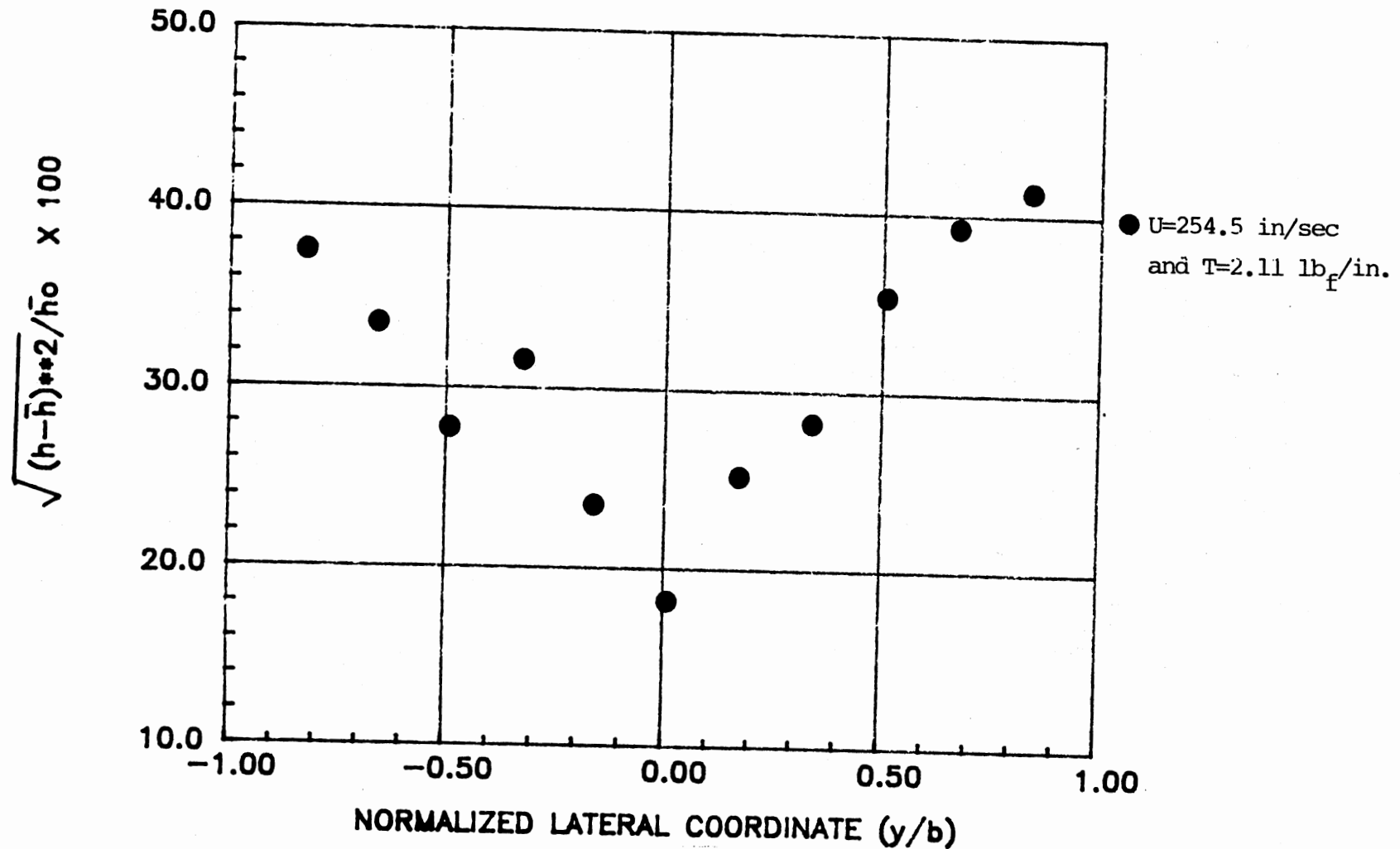


Figure 35. Lateral RMS Fluctuation of Air Film Thickness  
 in Constant Gap Region (White Polypropylene  
 Web)

in Figure 34 for the metallized web.

In order to reduce the possibility of the data being affected by the blemishes on the web surface, each time a new web was used for recording not more than five data points along the width of the web at five different prescribed locations. The data was recorded in the following way. For the first time, with a new web, probe was positioned at  $y/b=0$  (i.e. at the center of the web's width), now data will be recorded at this location which has the smallest possibility of being affected by the blemishes on the web surface. Then with the same web on, probe was traversed on both sides of the web width across the center line at five different locations while the data was recorded at each corresponding probe location. For the second time, again putting a new web on, probe was positioned at a new location i.e. at  $y/b=0.333$ , now this point will have the smallest possibility of being affected by surface blemishes and so on.

## CHAPTER IV

### CONCLUSIONS AND RECOMMENDATIONS

#### 4.1 Conclusions

Based upon the experimental measurements, the following conclusions may be drawn:

1. Experimental data for the air film thickness in constant gap region at different web velocities and tension levels seem to be in good agreement with the theoretically predicted values. The air gap thickness was found to be modelled correctly as regard the effect of changes in velocity and effective tensions are concerned (see Figures 17 and 18). The functional variation of the air film thickness  $h_0$ , as predicted by theory seems to retain its form in all experimental data, but the measured air film thickness is higher than its corresponding theoretical value. A modified equation for determining the air film thickness in constant gap region is presented and compared with data (see Figures 19 and 20). This discrepancy may be in part because of neglect of inertial effects in the model or due to the additional pressure rise in the vicinity of the nip region (Figure 1), due to the deceleration of the incoming air in that

region.

2. Measurements of the air film thickness along the angle of wrap of the web shows that constant gap region exists only approximately central 70% of the total statically determined wrap angle while the theory suggests that entire region under the wrap possesses a constant air gap. One reason for this reduced constant gap region is might be due to the existence of inlet and exit transitory regions in the presence of relative motion between the web and the roller. A dynamic measurement of the wrap angle would probably give more accurate measure of the azimuthal extent of the constant gap region (see Figures 22 and 23).

3. Experimental measurements shows that the lateral extent of the constant gap region is only central 50% of the total width of the web. Measurements also show that towards the outer edges of the web, because of the side leakage of air, the air film thickness reduces and thus web gets closer to the roller in that region (see Figures 24 and 25).

4. Figure 25 shows a relatively sharp reduction in the air film thickness when the experiment was performed on a roller surface which was worn-out in a circumferential but very small, grooved like pattern. This shows that grooved roller enhances the leaking ability of the entrapped air. This further suggests that the present measuring technique can also be used in

evaluating the effect of differently grooved rollers on entrapped air film.

5. The comparison of experimental lateral air film thickness data with theoretically predicted values suggests that bending of web cannot be approximated as a bending of flat plate for "edge effect analysis" in the web equilibrium equation and should be approximated as the bending of a cylindrical shell.

6. The rms fluctuation of the web (see Figures 34 and 35) shows that the outer edges of the web fluctuate with higher amplitudes than at the center. This indicates the complexity of the out of plane oscillation and may be attributed to any one of the following: a) Flapping of the web edges and/or b) Banking of the web as it passes over the roller. Determining the mode shapes would obviously require multi-probe measurements in order to obtain the required phase data.

#### 4.2 Recommendations For Future Work

1. Investigation regarding the presence of air inertial effects like the dynamic component in the pressure term i.e.  $1/2\rho V^2$  could be further substantiated by performing same experiments on machines capable of running webs at speeds up to 10,000 fpm and at lower tension levels.

2. As the present technique works on the principle of transmission and reflection of light rays and thus

probe's output signal partially depends on the reflectivity of the target surface. The use of automatic reflection compensator is highly recommended for future work because the reflectivity and gloss of the moving web surface changes by substantial amounts after a few runs.

3. It is recommended for the future work to incorporate some means in the test set-up in order to allow probe to scan all the three regions of web-roller interaction, which are 1. Inlet region 2. Constant gap region 3. Exit region. Such study will provide an indepth understanding about the behaviour of entrapped air in the respective regions.

4. Future work should involve better and accurate methods for applying, and measuring tensions and velocities.

5. As it has been observed that grooved rollers are effective in reducing the thickness of entrapped air film between the web and the roller. It is recommended for the future work to study the effect of differently grooved rollers on the entrapped air film.

6. The present experimental work employed only non-porous webs while web handling processess involve porous webs as well. It is recommended for the future work to use porous webs like paper web, in order to evaluate the effect of tranverse flow (because of porous webs-w component of velocity will be present) on the entrapped air film.

7. In order to widen the scope of validation of mathematical model, it is recommended that experiments be performed with the web materials having different elastic properties, varying widths and thicknesses and on supporting rollers of different radii.

8. Two point measurements for phase determination is recommended for future work in order to more fully understand the temporal oscillations of the web.

#### A SELECTED BIBLIOGRAPHY

1. Knox, K. L. and Sweeney, T. L., "Fluid EFFECTS Associated with Web Handling." Ind. Eng. Chem. Process, 10, 201-205 (1971).
2. Tajuddin, "Mathematical Modelling of Air Entrainment in Web Handling Applications". M.S. thesis, Oklahoma State University, (1987).
3. Timoshenko, S., Theory of Plates and Shells, McGraw Hill Book Company, Inc., New York, 1940.
4. Gross, W. A., Gas Film Lubrication, John Wiley and Sons, Inc., New York, 1962.
5. CRC Handbook of Tables for Applied Engineering Science, CRC Press.
6. Bendat, S. J., and Piersol, A. G., Random Data: Analysis and Measurement Procedures, John Wiley and Sons, Inc., New York, 1971.



## APPENDICES

APPENDIX A

DESCRIPTION OF THE FIFE ELECTRO MECHANICAL  
GUIDE SYSTEM

The web-moving machine has a fine electro-mechanical guiding system as shown on the left of Figure 36. The guiding system utilizes Fife A9 signal processor, one infra-red sensor, an electro-mechanical actuator and a guide structure.

The sensor contains light emitting diodes that emit infra-red light. This light is received across the gap of the sensor by a solar cell. The current conducted by the solar cell depends on the amount of light striking the cell. The amount of light from the LED's available to strike the cell is governed by the lateral position of the web in the sensor. As the web moves laterally in the sensor, the current being conducted by the cell varies due to the change in light. With a web at a certain point (called a guide point), the current is stable at a definite value (called the null point). The A9 signal processor detects any difference between the current due to the actual web position and the current at the null point. If there is a difference, the signal processor outputs a voltage signal to the DC-servo motor on the actuator assembly. The servo motor rotates a precision ball screw that causes the displacement-type guide structure to move, bringing the web back to the guide point. The speed of correction is proportional to the amount of web position error detected.

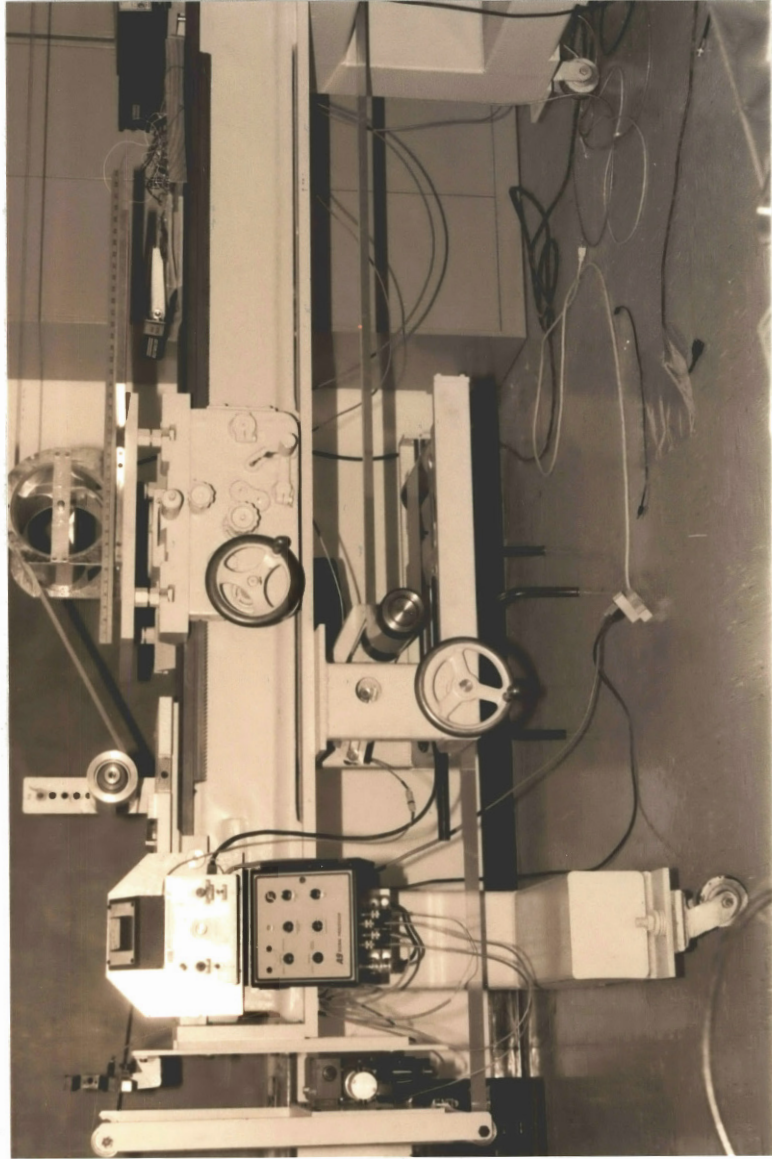


Figure 36. Photograph of Web-Moving Machine

**APPENDIX B**

**DESCRIPTION OF THE CALIBRATION MICROMETER**

The calibration micrometer as shown in Figure 37 comprises of the following components:

1. Main Slider Block (Figures 38)
2. V-Shaped Rectangular Block (Figures 39)
3. Slider-Key With Tapered Slot (Figure 40)

The combined calibration mechanism works as follows:

The Fotonic sensor was mounted securely on a V-shaped rectangular block through an eye-socket. The block was then flushed to a tapered slot on the slider key with a small rod. In order to move the probe by very small but known steps, the slider-key was connected to a precisely-bored and threaded hole on the body of main slider block via a positioning screw. So, as the screw rotates, clockwise or counter clockwise, the key slides in or out by the discrete amounts, dictated by the rotation of screw. Hence the amount of rise of small rod along the tapered slot will be transferred as the corresponding perpendicular movement of the probe.  $90^{\circ}$  rotation of positioning screw will cause probe to move 0.0001 inches perpendicularly.



Figure 37. Photograph of Calibration Micrometer

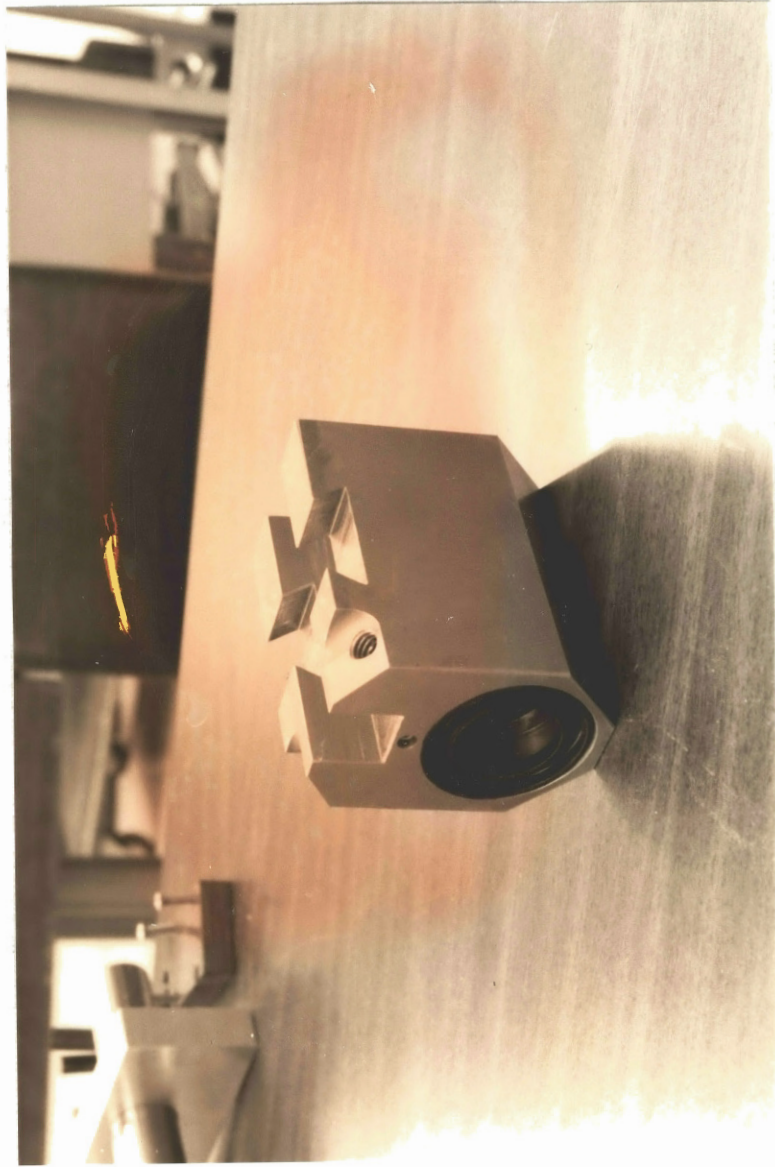


Figure 38. Main Slider Block





Figure 39. V-Shaped Rectangular Block



Figure 40. Slider Key with Tapered Slot

APPENDIX C

SPECIFICATIONS OF THE WEB MATERIALS

Webs of two different materials, provided by Mobil Chemical Company, New York, were used in all experimental work. One was a three layer Polypropylene A/B/C co-extrusion with vacuum deposited aluminum on one surface. The second was a three layer polypropylene A/B/A co-extrusion to which an additional white colored anti-static coating was applied on both surface. Other specifications of both of these materials, as provided by the manufacturer, are included in Tables II and III.

TABLE II  
 SPECIFICATIONS OF THE WHITE POLYPROYLENE WEB  
 AS PROVIDED BY THE MANUFACTURER

PROPERTIES	UNITS	TYPICAL VALUE	
Designation		250 ASW	
Gauge	Mil	1.7	
Yield	sq.in/lb	24,400	
Gloss;Gardner 45°		100	
Light Transmission	%	30	
Modulus	lbs/in <sup>2</sup>	MD	230,000
		TD	350,000
Tensile Strength	lbs/in <sup>2</sup>	MD	14,000
		TD	20,000
Coefficient of friction	acrylic/acrylic	0.25	
Flexural Rigidity		MD	1.07x10 <sup>-4</sup>
		TD	1.63x10 <sup>-4</sup>
Extensional Rigidity	lb/in	MD	391
	lb/in	TD	595

TABLE III  
 SPECIFICATIONS OF THE METALLIZED WEB AS  
 PROVIDED BY THE MANUFACTURER

PROPERTIES	UNITS	TYPICAL VALUE	
Designation		140 Metallite	
Gauge	Mil	1.40	
Yield	in <sup>2</sup> /lb	22,000	
Modulus	lb/in <sup>2</sup>	MD	350,000
		TD	550,000
Tensile Strength	lb/in <sup>2</sup>	MD	16,000
		TD	32,000
Coefficient of Friction	Film/Film	0.35	
	Film/Metal	0.25	
Light Transmission	%	2.0	
Flexural Rigidity		MD	9.12x10 <sup>-5</sup>
		TD	1.43x10 <sup>-4</sup>
Extensional Rigidity	lb/in	MD	490
		TD	770

APPENDIX D

COMPUTER PROGRAM LISTINGS

```

/*
*****-
*****

Instrument and Language : The following program is
written in TURBO-C language and works on TI-professional
computer on to which DT-2805 A/D, 12-bit board has been
installed.

Purpose : This program reads time varying voltage signal
from DT-2805 A/D board. The input to this board is the
analog signal from any process. The program than
digitizes the analog signal in real time at the sampling
rate specified by the user. It than calculates and saves
the average and rms values of the data in file
'AVRMS.DAT' and time history of the signal in file
'DATPONT.DAT'.

Structure : The function main(), has a menu showing
different options. When the user select any option, it
calls the necessary routines in order to execute that
option.

*****-
*****
*/

#include <stdio.h >
#include <string.h>
#include <dos.h>
#include <math.h>
#include <conio.h>

/*
=====
=====
*/

#define MAXLINE 80
#define MAX 2000

int _stack=100000;
unsigned char clock1[9], clock2[9];

/*
=====
=====
Function : main.
Purpose : To execute diferent options.

=====
=====
*/

```



```

main()
{
    int      i, j, n, nconv,
            quit, jk, l, mj, ikk, ijk, kn, ntime,
            delay1, iik, jjk;
    long     m;
    int      n_chan, start_chan, end_chan, period,
            gain, delay2 ;
    int      ad_lo[MAX], ad_hi[MAX], my, min, jhk, again ;
    double   tol, sens[MAX], value, result, avgres, per,
            tim;
    double   rmsval1, rmsval2, rms, wosplice[MAX],
            wodcbias[MAX];
    char     answer, message[MAXLINE], cal;
    char     time1[30], time2[30], osc;
    FILE     *fout;

    strcpy(message, " ");
    strcpy(time1, " ");
    strcpy(time2, " ");
    quit     = 0;
    start_chan = 7;
    end_chan  = 7;
    period   = 1500;
    n = 2000;
    nconv = n*1;
    n_chan = 1;
    jk = 0;
    ntime = 1;
    gain = 0;
    /*      Board Initialization      */
    clear_board();
    set_clock(period);
    set_ad_param(nconv, start_chan, end_chan, gain);
    printf("\n      Enter outer delay      \n");
    scanf("%d", &delay1);
    printf("\n      Enter inner delay      \n");
    scanf("%d", &delay2);
    printf("\n      Enter splice off-set for
            this run.      \n");
    scanf("%lf", &tol);
    printf("\n Type 'T' if running for calibration
            \n");
    scanf("%c", &cal);
    while( ! quit)
    {
        scroll(24);
        printf("      Select Any One Of The
            Following Options \n");
        printf("      <C>lear board      \n");
        printf("      <N>umber Of Data Points : %d \n", n);
    }
}

```

```

printf("      <P>eriod or Sampling Time      : %d
      \n",period);
printf("      <R>ead Voltage                    \n");
printf("      <A>verage and RMS values          \n");
printf("      <V>iew Digitized Signal           \n");
printf("      <S>ave Data                        \n");
printf("      <L>ine Velocity Store Points:  %d
      \n",ntime);
printf("      <E>xit                            \n\n");
printf("      Clock Time Before Sampling = %s
      \n",time1);
printf("\n      Clock Time After Sampling = %s
      \n",time2);

printf("%s",message);
strcpy(message," ");
scroll(10);
scanf("%s",&answer);

switch(answer){

    case 'c':
    case 'C':

        clear_board();
        printf("%c",answer);
        set_clock(period);
        printf("%c",answer);
        set_ad_param(nconv, start_chan, end_chan,
            gain);
        break;

    case 'n':
    case 'N':

        printf("Number of Data Points = ");
        scanf("%d",&n);
        if( n > MAX ) {
            n = MAX;
            strcpy(message,"N must be less than
            MAX");
        }
        nconv = 1*n;
        set_ad_param(nconv, start_chan, end_chan,
            gain);
        break;

    case 'p':
    case 'P':

        printf("Sampling Period = ");
        scanf("%d",&period);
        set_clock(period);
        per = (float) *(&period) * 0.0000025;
        break;

```

```

case 'l':
case 'L':

    printf("Number of data points to be stored=
    ");
    scanf("%d",&ntime);
    break;

case 'r':
case 'R':

    for ( ijk=0; ijk <delay1; ijk++)
    {
        getclk(clock1);
        read_ad(nconv,ad_lo,ad_hi);
        getclk(clock2);
        stptime(time1,4,&clock1[4]);
        stptime(time2,4,&clock2[4]);
        result = 0.0;
        rmsvall = 0.0;
        rmsval2 = 0.0;
        avgres = 0.0;
        rms = 0.0;
        iik=0;
        jjk=0;
        kn=1;
        for( i=0; i<n; ++i)
        {
            for( j=0; j<n_chan; ++j)

            value = ad_hi[i*n_chan+j]*256.0 +
                ad_lo[i*n_chan+j];
            sens[i] = 10*(2.0*value/4096.0
                -1.0);
            /* sens[i] = 10 * (value/4096.0);
            for unipolar mode */
            if (( cal != 't') && ( cal != 'T'))
            {
                if ((sens[i] > sens[0]-tol) &&
                    (sens[i] < sens[0]+tol))

                {

                    result = result + sens[i];
                    rmsvall = rmsvall + (sens[i] *
                        sens[i] );
                    kn=kn+1;
                    wosplce[iik]=sens[i];
                    iik=iik+1;
                }
            }
        }
    }
    else / if (( cal =='T')|| ( cal == 't'))

```

```

    {
        result= result +sens[i];
        rmsvall=rmsvall+(sens[i]*sens[i]);
        kn=kn+1;
    }
} /* for j */
/* for i */

    avgres = result/kn;
    rmsval2 = (rmsvall/kn);
    rms = sqrt(rmsval2);
for (min=0; min<iik; min++)
{
    wodcbias[min]=wospllice[min]-rms;
}

case 'a':
case 'A':

    printf("\n RMS VALUE = %f \n ", rms);
    printf("\n AVG VALUE = %f \n ",avgres);

case 's':
case 'S':

    fout = fopen("avrms.dat","a");
    jk = jk +1;
    fprintf(fout," %d ",jk);
    fprintf(fout," %f %f ",avgres,rms);
    fprintf(fout,"\n");
    fclose(fout);
    fout = fopen("datpont.dat","w");
    for( i=0; i<ntime ; i++)
    {
        tim =(float) period*0.0000025*(float) i ;
        fprintf(fout," %f ",tim);
        for( j=0; j<n_chan; ++j)
        {
            fprintf(fout," %f ",sens[i]);
        }
        /*for j */
        fprintf(fout,"\n");
        /*for i */
        fclose(fout);
        if ((osc != 'f') && (osc != 'F'))
            iik=1;
        fout=fopen("fluctut","w");
        for (i=0;i<iik;i++)
        {
            fprintf(fout,"%d %lf %lf ",
                i, wospllice[i], wodcbias[i]);
            fprintf(fout,"\n");
        }
        fclose(fout);
        for (ikk=0; ikk<delay2; ikk++)

```

```

        {
        }
    }
    break;

    case 'e':
    case 'E':

        quit = 1;
        break;

    default :

        strcpy (message,"Please enter one of the
                valid options");

        }/* switch */
    }/* while #1 */

    scroll(24);
    exit();

}    /* end of Function main */

/*
=====
Interactive routines
=====
*/

scroll(n)
int n;
{
    int i;
    for( i=0; i<n; ++i)
        printf("\n");
}/* scroll */

/*
=====
Board functions
=====
*/

/* Define registers */

#define CMDREG    0x101 /*Command register */
#define STREG     0x101 /* Status register */
#define DATREG    0x100 /* Data register */

```

```

                /* Define Masks */

#define CMDMSK    0x4    /* Command mask */
#define REDMSK    0x5    /* Read mask */
#define WRTMSK    0x2    /* Write mask */

                /* Define commands */

#define C_RESET   0x0    /* Reset board */
#define C_CLEAR   0x1    /* Clear Errorr */
#define C_SCLOCK  0x3    /* Set internal clock */
#define C_SDA     0x9    /* Set d/a parameters */
#define C_SAD     0xd    /* Set a/d parameters */
#define C_RAD     0xe    /* Read a/d */
#define C_STOP    0xf    /* Stop board */
#define CONTINUOUS 0x20  /* Continuous mode */

/*
-----
-----

Function : clear_board.
Purpose  : To clear the board.

Parameters
None.

Variables
i          : Temporary variable to dump data.

Remarks
Have to call this function before using the board.

-----
-----

*/

clear_board()
{
    int i;
    outportb(CMDREG,C_STOP); /* Write stop command */
    i = inportb(DATREG);     /* Read data register and
                             ignore */
    while( !(CMDMSK & inportb(STREG))); /* Check status
                                         register */
    outportb(CMDREG,C_RESET); /* Write reset command */
    while( !(REDMSK & inportb(STREG)));
    i = inportb(DATREG);     /* Read data register and
                             ignore */ } /*

end of Function clear_board() */

/*
-----
-----

```

-----  
 Function : set\_clock.  
 Purpose : Set the clock period.

Parameters  
 period : Clock period in ....

Variables  
 lo\_byte : Temporary variable, holds low byte of period.  
 hi\_byte : Temporary variable, holds high byte of period.

Remarks  
 Must be used before calling the continuous a/d and d/a functions.

-----  
 -----  
 \*/  
 set\_clock(period)  
 long period;  
 {  
   int lo\_byte, hi\_byte;  
   hi\_byte = period/256;  
   lo\_byte = period - hi\_byte\*256;  
   while(!(CMDMSK & inportb(STREG))); /\* Check status  
   register \*/  
 outportb(CMDREG,C\_SCLOCK); /\* Write, set clock  
   command \*/     while(WRTMSK  
 & inportb(STREG));  
   outportb(DATREG,lo\_byte); /\* Output low byte \*/  
   while(WRTMSK & inportb(STREG));  
   outportb(DATREG,hi\_byte); /\* Output high byte \*/  
 } /\* end of Function set\_clock() \*/  
 /\*

-----  
 -----  
 Function : set\_ad\_param.  
 Purpose : Set the analog to digital parameters.

Parameters  
 nconvr : Number of conversions.  
 start\_chan1 : Starting channel.  
 end\_chan1 : End channel.  
 gain : Code for gain in a/d conversion.

Variables  
 lo\_byte : Temporary variable, holds low byte of

hi\_byte : period.  
: Temporary variable, holds high byte of  
period.

#### Remarks

Must be used before calling the a/d functions.

```

-----
-----
*/

set_ad_param(nconvr,start_chanl,end_chanl,gain)
int nconvr, start_chanl, end_chanl, gain;
{
    int lo_byte, hi_byte;
    while(!(CMDMSK & inportb(STREG)));/* Check status
                                     register */
    outportb(CMDREG,C_SAD);/* Write, set a/d parameters
                             */
    while(WRTMSK & inportb(STREG));
    outportb(DATREG,gain); /* Specify gain */
    while(WRTMSK & inportb(STREG));
    outportb(DATREG,start_chanl); /* Specify start
                                   channel number */
    while(WRTMSK & inportb(STREG));
    outportb(DATREG,end_chanl); /* Specify end chanel
                                   number */
    hi_byte = nconvr/256;
    lo_byte = nconvr - hi_byte*256;
    while(WRTMSK & inportb(STREG));
    outportb(DATREG,lo_byte); /* Output low byte */
    while(WRTMSK & inportb(STREG));
    outportb(DATREG,hi_byte); /* Output high byte */
} /* end of Function set_ad_param() */

/*
-----
-----

```

Function: float read\_ad\_immed().

Purpose : Get the value from the specified channel,  
and return the actual voltage.

#### Parameters

read\_ad\_immed : The value in volts.  
gain : Code for gain in a/d conversion.  
channel : Channel to be read.

#### Variables

lo\_byte : Temporary variable holds the low byte of  
the conversion.  
hi\_byte : Temporary variable holds the high byte of



Value : the conversion.  
: Used to calculate the volts.

#### Remarks

Must call the function `set_ad` before using this function. Also remember to declare `read_ad_immed()` in the calling routine as a float.

```

-----
-----
*/

float read_ad_immed(gain,channel)
int gain, channel;
{
    int lo_byte, hi_byte;
    float value;
    while(!(CMDMSK & inp(STREG))); /* Check status
                                register */
    outp(CMDREG,C_RADIMM); /* Write, read a/d immediate
                           command */
    while(WRTMSK & inp(STREG));
    outp(DATREG,gain); /* Specify gain code */
    while(WRTMSK & inp(STREG));
    outp(DATREG,channel); /* Specify channel */
    while(!(REDMSK & inp(STREG)));
    lo_byte = inp(DATREG); /* Read low byte */
    while(!(REDMSK & inp(STREG)));
    hi_byte = inp(DATREG); /* Read high byte */
    value = hi_byte*256.0 + lo_byte; /* Find equivalent
                                    voltage */
    value = 10.0*(2.0*value/4096.0 - 1.0);
    return(value);
}/* end of Function read_ad_immed() */

/*
-----
-----

```

Function : `read_ad`.

Purpose : Get the value from the specified channel.

#### Parameters

`n` : Number of conversions  
`ad_lo` : Array with low byte of a/d value.  
`ad_hi` : Array with high byte of a/d value .

#### Variables

`i` : Temporary variable.

#### Remarks

Must call the function set\_clock and set\_ad before using this function.

```
-----  
-----  
*/  
  
read_ad(n,ad_lo,ad_hi)  
int n, ad_lo[], ad_hi[];  
{  
    int i;  
    while(!(CMDMSK & inportb(STREG)));  
    outportb(CMDREG,C_RAD); /* 20 0e */  
    for( i=0; i<n; ++i)  
    {  
        while( !(REDMSK & inportb(STREG)) );  
        ad_lo[i] = inportb(DATREG); /* Read low byte */  
        while( !(REDMSK & inportb(STREG)) );  
        ad_hi[i] = inportb(DATREG); /* Read high byte */  
    } /* for i */  
} /* end of Function read_ad() */  
  
/*
```

2  
VITA

MOHAMMAD SOHAIL BASHEER

Candidate for the Degree of  
Master of Science

Thesis: AN EXPERIMENTAL STUDY OF AIR ENTRAINMENT IN WEB  
HANDLING APPLICATIONS

Major Field: Mechanical Engineering

Biographical:

Personal Data: Born in Karachi, Pakistan, December  
23, 1961, the son of Mr. Mohammad Basheer Uddin  
and Mrs. Zainub Basheer.

Education: Graduated from Government Adamjee Science  
College, Karachi, Pakistan, in July 1978;  
received Bachelor of Engineering Degree from  
N.E.D University of Engineering and Technology  
in March 1985; completed requirements for the  
Master of Science Degree at Oklahoma State  
University in July, 1988.

Professional Experience: Research Assistant at  
Oklahoma State University, School of Mechanical  
and Aerospace Engineering, June, 1986 - present.